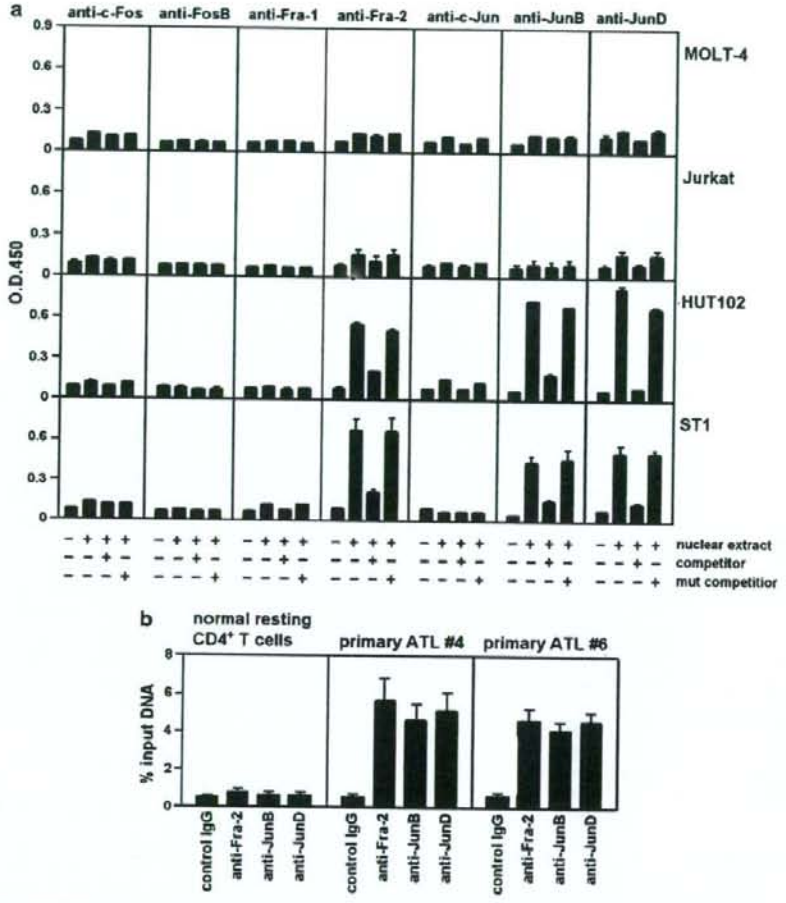

Figure 4 Specific binding of Fra-2, JunB and JunD to the AP-1 site in the CCR4 promoter. (**a**) NoShift assay. Nuclear extracts were prepared from two control T-cell lines (MOLT-4 and Jurkat) and two adult T-cell leukemia (ATL) cell lines (HUT102 and ST1). Nuclear proteins that bound to the biotinylated AP-1 site oligonucleotide (TGGGAAATGACTAAGAATCAT) were captured on an avidin-coated plate and detected by anti-c-Fos, anti-FosB, anti-Fra-1, anti-Fra-2, anti-c-Jun, anti-JunB or anti-JunD, as indicated. Specificity was determined by adding unlabeled probe (competitor; TGGGAAATGACTAAGAATCAT) or mutant probe (mut competitor; TGGGAAATGTCAAAGAATCAT; differences underlined). Each bar represents the mean ± s.e.m. from three separate experiments. (**b**) Chromatin immunoprecipitation (ChIP) assay. Chromatins from normal CD4+ T cells from healthy donors (purity, >96%) and primary ATL cells from two patients (leukemic cells, >90%) were immunoprecipitated with anti-Fra-2, anti-JunD or control IgG. The amounts of precipitated DNA relative to total input DNA were quantified by real-time PCR for the CCR4 promoter region containing the AP-1 site. Each bar represents the mean ± s.e.m. from three separate experiments.

Identification of downstream target genes of the Fra-2/JunD heterodimer in ATL cells

To identify the target genes of Fra-2 in ATL cells, we compared the gene expression profiles of ATL-derived ST1 cells transfected with Fra-2 siRNA or control siRNA using the Affymetrix high-density oligonucleotide microarray. As summarized in Figure 6a, at least 49 genes were downregulated more than threefold by Fra-2 siRNA. The classification of these genes according to their biological functions shows that Fra-2 promotes the expression of genes involved in signal transduction (10 genes), protein biosynthesis and modification (8 genes) and transcription (6 genes); it also stimulates the expression of 10 genes of unknown function. Most notably, the list includes the proto-oncogenes c-Myb, BCL-6 and MDM2 (Oh and Reddy, 1999; Pasqualucci *et al*., 2003; Vargas *et al*., 2003). As shown in Figure 6b, RT–PCR analysis verified that not only Fra-2 siRNA but also JunD siRNA downregulated these proto-oncogenes in two ATL cell lines. Therefore, c-Myb, BCL-6 and MDM2 are the downstream target genes of the Fra-2/JunD heterodimer in both cell lines. This prompted us to examine the expression of c-Myb, BCL-6 and MDM2 in freshly isolated primary ATL cells by

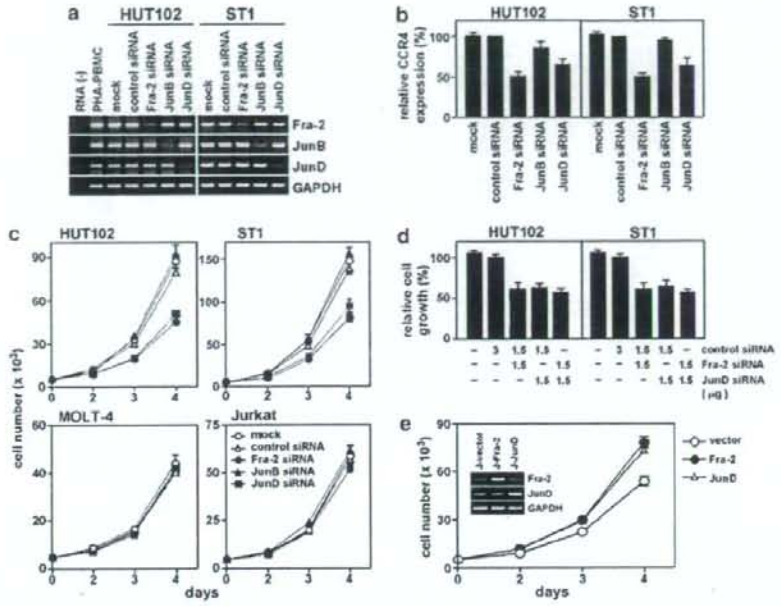

Figure 5 Dominant role of Fra-2/JunD in CCR4 expression and cell proliferation in adult T-cell leukemia (ATL). (**a**) Reverse transcription (RT)–PCR analysis to determine the effect of siRNAs. HUT102 and ST1 were transfected with control siRNA or siRNA for Fra-2, JunB or JunD. After 48 h, total RNA was prepared. The representative results from three separate experiments are shown. (**b**) Real-time RT–PCR analysis for CCR4 expression. HUT102 and ST1 were transfected with control siRNA or siRNA for Fra-2, JunB or JunD. After 48 h, total RNA was prepared and real-time RT–PCR was performed for CCR4 and 18S ribosomal RNA (an internal control). Data are presented as the mean ± s.e.m. of three separate experiments. (**c**) Effect of siRNAs on cell growth. HUT102, ST1, MOLT-4 and Jurkat were transfected with control, Fra-2, JunB and JunD siRNAs and cultured in a 96-well plate at 0.5×10^4 cells per well. At the indicated time points, viable cell numbers were determined using a FACSCalibur by gating out cells stained with propidium iodide. Data are shown as the mean ± s.e.m. of three separate experiments. (**d**) Effect of double knockdown of Fra-2 and JunD on cell growth. HUT102 and ST1 were transfected with control, Fra-2 and JunD siRNAs as indicated and cultured in a 96-well plate at 0.5×10^4 cells per well. At 4 days, viable cell numbers were determined on a FACSCalibur by gating out dead cells stained with propidium iodide. Data are shown as the mean ± s.e.m. of three separate experiments. (**e**) Effect of stable expression of Fra-2 and JunD on cell growth. Jurkat cells were transfected with a control IRES-EGFP expression vector or an IRES-EGFP expression vector for Fra-2 or JunD. Stable transfectants expressing green fluorescence protein were sorted and cultured in a 96-well plate at 0.5×10^4 cells per well. At the indicated time points, viable cell numbers were determined on a FACSCalibur by gating out dead cells stained with propidium iodide. Data are shown as the mean ± s.e.m. of three separate experiments.

RT–PCR. As shown in Figure 6c, we indeed detected the constitutive expression of c-Myb, BCL-6 and MDM2 at high levels in primary ATL cells. In sharp contrast, normal resting $CD4^+$ T cells hardly expressed these proto-oncogenes.

Discussion

The AP-1 transcription factors function as homodimers or heterodimers formed by Jun (c-Jun, JunB and JunD), Fos (c-Fos, FosB, Fra-1 and Fra-2) and the ATF family proteins (Shaulian and Karin, 2002; Eferl and Wagner, 2003). Most of them are rapidly and transiently induced by extracellular stimuli that trigger the activation of the Janus kinase (JNK), extracellular signal regulated protein kinases 1 and 2 (ERK1/2) or p38 mitogen-activated protein (MAP) kinase pathways (Shaulian and Karin, 2002; Eferl and Wagner, 2003). The AP-1 family is known to be involved in cellular proliferation, oncogenesis and even tumor suppression, depending on the combination of AP-1 proteins and the cellular context (Shaulian and Karin, 2002; Eferl and Wagner, 2003). Previously, by using the AP-1 site of the IL-8 promoter, Mori *et al.* demonstrated a strong Tax-independent expression of JunD in primary ATL cells (Mori *et al.*, 2000). In the present study, we have shown that Fra-2 is constitutively expressed at high levels in primary ATL cells (Figure 2a). Furthermore, except for JunB and JunD, other members of the AP-1 family are mostly negative in primary ATL cells (Figure 2a). Therefore, as demonstrated in the present study, the Fra-2/JunD and Fra-2/JunB heterodimers may be the major AP-1 factors constitutively active in primary ATL cells.

It has been shown that HTLV-1 Tax induces the expression of various AP-1 family members such as c-Fos, Fra-1, c-Jun and JunD (Nagata *et al.*, 1989; Iwai *et al.*, 2001). We indeed observed the expression of

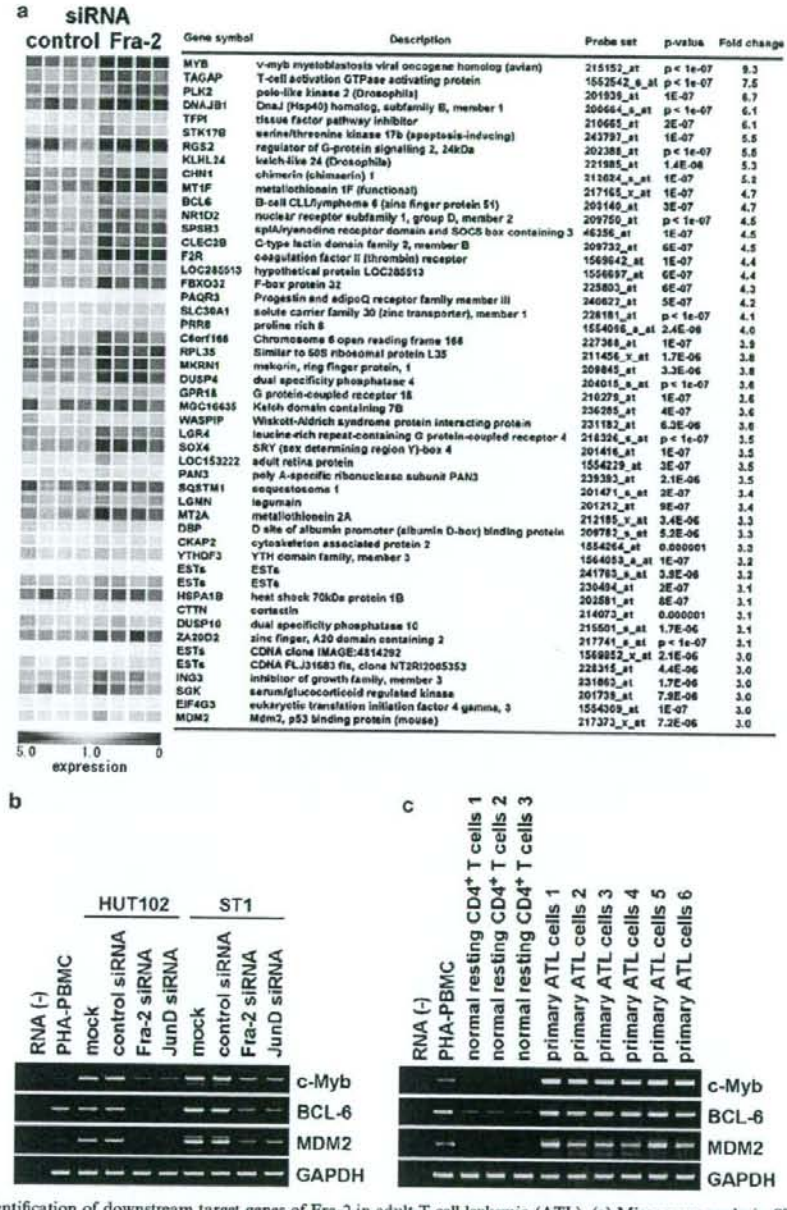

Gene symbol	Description	Probe set	p-value	Fold change
MYB	v-myb myeloblastosis viral oncogene homolog (avian)	215152_at	p< 1e-07	9.3
TAGAP	T-cell activation GTPase activating protein	1552542_a_at	p< 1e-07	7.5
PLK2	polo-like kinase 2 (Drosophila)	201939_at	1E-07	6.7
DNAJB1	DnaJ (Hsp40) homolog, subfamily B, member 1	200664_s_at	p< 1e-07	6.1
TFPI	tissue factor pathway inhibitor	210665_at	2E-07	6.1
STK17B	serine/threonine kinase 17b (apoptosis-inducing)	243797_at	1E-07	5.5
RGS2	regulator of G-protein signaling 2, 24kDa	202388_at	p< 1e-07	5.5
KLHL24	kelch-like 24 (Drosophila)	221585_at	1.4E-06	5.3
CHN1	chimerin (chimaerin) 1	213624_s_at	1E-07	5.2
MT1F	metallothionein 1F (functional)	217165_x_at	1E-07	4.7
BCL6	B-cell CLL/lymphoma 6 (zinc finger protein 51)	203140_at	3E-07	4.7
NR1D2	nuclear receptor subfamily 1, group D, member 2	209750_at	p< 1e-07	4.5
SPSB3	spIA/ryanodine receptor domain and SOCS box containing 3	46356_at	1E-07	4.5
CLEC2B	C-type lectin domain family 2, member B	209732_at	6E-07	4.5
F2R	coagulation factor II (thrombin) receptor	1569642_at	1E-07	4.4
LOC285513	hypothetical protein LOC285513	1556697_at	6E-07	4.4
FBXO32	F-box protein 32	225803_at	6E-07	4.3
PAQR3	Progestin and adipoQ receptor family member III	240627_at	5E-07	4.2
SLC30A1	solute carrier family 30 (zinc transporter), member 1	226181_at	p< 1e-07	4.1
PRR8	proline rich 8	1554056_a_at	2.4E-06	4.0
C6orf166	Chromosome 6 open reading frame 166	227368_at	1E-07	3.9
RPL35	Similar to 60S ribosomal protein L35	211456_x_at	1.7E-06	3.8
MKRN1	makorin, ring finger protein, 1	209845_at	3.3E-06	3.8
DUSP4	dual specificity phosphatase 4	204015_s_at	p< 1e-07	3.6
GPR18	G protein-coupled receptor 18	210279_at	1E-07	3.6
MGC16635	Kelch domain containing 7B	236265_at	4E-07	3.6
WASPIP	Wiskott-Aldrich syndrome protein interacting protein	231182_at	6.3E-06	3.6
LGR4	leucine-rich repeat-containing G protein-coupled receptor 4	218326_s_at	p< 1e-07	3.5
SOX4	SRY (sex determining region Y)-box 4	201416_at	1E-07	3.5
LOC153222	adult retina protein	1554229_at	3E-07	3.5
PAN3	poly A-specific ribonuclease subunit PAN3	239383_at	2.1E-06	3.5
SQSTM1	sequestosome 1	201471_s_at	2E-07	3.4
LGMN	legumain	201212_at	9E-07	3.4
MT2A	metallothionein 2A	212185_x_at	3.4E-06	3.3
DBP	D site of albumin promoter (albumin D-box) binding protein	209782_s_at	5.3E-06	3.3
CKAP2	cytoskeleton associated protein 2	1554264_at	0.000001	3.3
YTHDF3	YTH domain family, member 3	1564053_a_at	1E-07	3.2
ESTs	ESTs	241783_s_at	3.5E-06	3.2
ESTs	ESTs	230494_at	2E-07	3.1
HSPA1B	heat shock 70kDa protein 1B	202581_at	8E-07	3.1
CTTN	cortactin	214073_at	0.000001	3.1
DUSP10	dual specificity phosphatase 10	215501_s_at	1.7E-06	3.1
ZA20D2	zinc finger, A20 domain containing 2	217741_s_at	p< 1e-07	3.1
ESTs	CDNA clone IMAGE:4814292	1569852_x_at	2.1E-06	3.0
ESTs	CDNA FLJ31683 fis, clone NT2RI2005353	228315_at	4.4E-06	3.0
ING3	inhibitor of growth family, member 3	231863_at	1.7E-06	3.0
SGK	serum/glucocorticoid regulated kinase	201739_at	7.9E-06	3.0
EIF4G3	eukaryotic translation initiation factor 4 gamma, 3	1554309_at	1E-07	3.0
MDM2	Mdm2, p53 binding protein (mouse)	217373_x_at	7.2E-06	3.0

Figure 6 Identification of downstream target genes of Fra-2 in adult T-cell leukemia (ATL). (**a**) Microarray analysis. ST1 cells were transfected with control siRNA or Fra-2 siRNA. After 48 h, microarray analysis was performed using the Affymetrix GeneChip HG-U133 Plus 2.0 array. Four independent transfection samples were analysed for each group. Each column represents the expression level of a given gene in an individual sample. Red represents increased expression and blue represents decreased expression relative to the normalized expression of the gene across all samples. We computed the statistical significance level for each gene between the Fra-2-knockdown group and the control group with a mean fold change of > 3 by the *t*-test ($P<10^{-5}$). (**b**) Reverse transcription (RT)–PCR analysis. HUT102 and ST1 cells were transfected with control siRNA or siRNA for Fra-2 or JunD. After 48 h, the expression of c-Myb, BCL-6, MDM2 and GAPDH was determined by RT–PCR. The representative results from three separate experiments are shown. (**c**) RT–PCR analysis. Normal CD4$^+$ T cells from healthy donors ($n=3$; purity, > 96%) and PBMC from ATL patients ($n=6$; leukemic cells, > 90%) were examined for the expression of c-Myb, BCL-6 and MDM2 by RT–PCR. The representative results from two separate experiments are shown.

various AP-1 family members in primary ATL cells (patient nos. 1 and 5) and in some ATL cell lines expressing Tax (Figures 2a and b). However, the constitutive expression of Fra-2, JunD and JunB in freshly isolated primary ATL cells and ATL cell lines is apparently independent from Tax expression (Figures 2a and b). This is further supported by the finding that CCR4-expressing HTLV-1-negative CTCL cell lines also constitutively express Fra-2, JunB and JunD at high levels (Figure 2). By using JPX-9, which is a subline of Jurkat carrying the HTLV-1 Tax gene under the control of the metallothionein gene promoter (Nagata *et al.*, 1989), we have also confirmed that Fra-2 is not inducible by Tax (data not shown).

The CCR4 promoter was potently activated by the Fra-2/JunB and Fra-2/JunD heterodimers (Figure 3a). Fra-2, JunB and JunD were also shown to bind specifically to the AP-1 site in the CCR4 promoter *in vitro* by the NoShift binding assays and *in vivo* by the ChIP assays (Figures 4a and b). By using the siRNA knockdown technique, however, only Fra-2 siRNA and JunD siRNA efficiently suppressed CCR4 expression and cell growth in ATL cell lines (Figure 5). On the other hand, JunB siRNA showed little such effect (Figure 5). Therefore, it is likely that, at least in terms of CCR4 expression and cell proliferation, the Fra-2/JunD heterodimer plays a more dominant role than the Fra-2/JunB heterodimer in ATL cells. It thus remains to be determined whether the Fra-2/JunB heterodimer has any specific functions in ATL.

The most striking finding in the present study is the aberrant expression of Fra-2 in primary ATL cells. Fra-2 expression is essentially absent in normal $CD4^+$ T cells under various conditions thus far examined (Figures 2a and c). Physiologically, Fra-2 is known to be expressed by various epithelial cells and in cartilaginous structures and has been shown to be required for efficient cartilage development (Karreth *et al.*, 2004). With regard to lymphoid cells, developing murine thymocytes were reported to express Fra-2 (Chen *et al.*, 1999). Previous studies have shown that individual homodimeric and heterodimeric AP-1 proteins have different functional properties and target genes (Shaulian and Karin, 2002; Eferl and Wagner, 2003). However, little is known about the target genes of Fra-2 and even less is known about the oncogenic role of Fra-2 in human malignancies. In this study, we have shown that CCR4 is the direct target gene of Fra-2 in association with JunD in ATL cells. Furthermore, we have shown that at least 49 genes are downregulated more than threefold in the ATL cell line ST-1 by Fra-2 siRNA (Figure 6). Among these genes, the proto-oncogenes c-Myb, BCL-6 and MDM2 (Oh and Reddy, 1999; Pasqualucci *et al.*, 2003; Vargas *et al.*, 2003) are further confirmed to be dependent on the Fra-2/JunD heterodimer and to be expressed at high levels in primary ATL cells (Figure 6). It remains to be seen whether the Fra-2/JunD heterodimer directly induces these proto-oncogenes or indirectly maintains their expression by promoting cell growth.

c-Myb is the genomic homologue of the avian myeloblastosis virus oncogene v-Myb. c-Myb is widely expressed in immature hematopoietic cells and also in various leukemias and carcinomas (Oh and Reddy, 1999; Shetzline *et al.*, 2004; Hess *et al.*, 2006). The target genes of c-Myb include the anti-apoptotic genes BCL-2 and $BCL\text{-}X_L$ and also c-Myc (Ramsay *et al.*, 2003). Thus, c-Myb may promote the survival of ATL cells via BCL-2 and $BCL\text{-}X_L$ (Galonek and Hardwick, 2006) and also cell cycle progression via c-Myc (Dang, 1999). BCL-6 was originally identified as the target gene of recurrent chromosomal translocations affecting 3q27 in non-Hodgkin's lymphoma. The expression of BCL-6 is frequently upregulated in diffuse large-cell lymphoma and follicular lymphoma through promoter substitution or somatic promoter point mutations (Ye *et al.*, 1993; Migliazza *et al.*, 1995; Chang *et al.*, 1996). Frequent expression of BCL-6 has also been reported in some T-cell lymphomas (Kerl *et al.*, 2001). The BCL-6 protein has been shown to exert cell-immortalizing and anti-senescence activities (Shvarts *et al.*, 2002; Pasqualucci *et al.*, 2003). Thus, BCL-6 may also inhibit apoptosis and promote cell cycle progression in ATL. The MDM2 protein is a negative regulator of p53 and suppresses p53-mediated cell cycle arrest and apoptosis (Vargas *et al.*, 2003). Elevated expression of MDM2 has been demonstrated in various types of human cancer (Rayburn *et al.*, 2005). Given that only a minor fraction of ATL cases have mutations affecting p53 (Cesarman *et al.*, 1992), the elevated expression of MDM2 may contribute to the functional downregulation of p53 in the majority of ATL cases.

CTCLs are a group of T-cell lymphomas derived from skin-homing memory T cells. CTCLs are not associated with HTLV-1 infection but resemble ATL and frequently express CCR4 (Ferenczi *et al.*, 2002; Kim *et al.*, 2005). Furthermore, CCR4 expression has been shown to be a consistent feature of the large-cell transformation of mycosis fungoides (Jones *et al.*, 2000). In the present study, we have shown that CTCL cell lines also express Fra-2, JunB and JunD at high levels (Figure 2b). Therefore, it is likely that aberrantly expressed Fra-2 in association with Jun proteins, particularly JunD, is also involved in CCR4-expression and cell proliferation in CTCLs.

In conclusion, we have shown that aberrantly expressed Fra-2 in association with JunD is responsible for CCR4 expression in ATL and is also likely to play an important role in ATL oncogenesis in part by inducing the expression of the proto-oncogenes c-Myb, BCL-6 and MDM2. Future studies are necessary to elucidate how the Fra-2/JunD heterodimer induces the expression of these proto-oncogenes and their individual roles in ATL oncogenesis. It also remains to be seen how ATL cells aberrantly express Fra-2 at high levels. Furthermore, the expression and function of Fra-2 in CTCLs remain to be determined.

Materials and methods

Cells

All the human T-cell lines used were described previously (Nagata *et al.*, 1989; Yamada *et al.*, 1996; Hata *et al.*, 1999;

Yoshie *et al*., 2002). Peripheral blood mononuclear cells (PBMC) were isolated from heparinized blood samples obtained from healthy adult donors and acute ATL patients with a high leukemic cell count (>90%) by using Ficoll-Paque (Amersham Biosciences Corp, Piscataway, NJ, USA). Normal $CD4^+$ T cells (purity, >96%) were further prepared from PBMC by negative selection using an IMagnet system (BD Pharmingen, San Diego, CA, USA). Activated $CD4^+$ T cells were prepared by stimulating $CD4^+$ T cells with anti-CD3 (clone HIT3a; BD Pharmingen) and anti-CD28 (clone CD28.2; BD Pharmingen) for 24 h. The preparation of naive $CD4^+CD45RA^+$ T cells and their polarization into Th1 and Th2 cells were performed as described previously (Imai *et al*., 1999). Primary ATL cells and normal resting $CD4^+$ T cells were used without culture for the experiments. This study was approved by the local ethical committee and written informed consent was obtained from each patient.

Transfection and luciferase assay

The major transcriptional start site (+1) of the human CCR4 gene was determined by the method of rapid amplification of cDNA 5′-ends and was found to be located 1797 bases upstream from the translation start codon (data not shown). To generate a promoter–reporter construct, the 1-kb promoter region of the human CCR4 gene (−983 to +25) was amplified from the genomic DNA by PCR using primers based on a GenBank genomic DNA sequence (accession no. NC_000003) and inserted into the reporter plasmid pGL3-Basic (Promega, Madison, WI, USA). Deletions and site-directed mutations were also performed using PCR. pGL3-2xAP-1 was constructed by introducing a sequence containing two copies of the AP-1 consensus binding site (TGATGACTCAGCCG-GAATGATGACTCAGCC) in front of a minimal CCR4 promoter pGL3 (−96/+25; Figure 1b). The coding regions of human FosB and GATA-3 were amplified from a cDNA library generated from phytohemagglutinin (PHA)-stimulated PBMC by PCR and cloned into the expression vector pSG5 (Stratagene, La Jolla, CA, USA). The coding region of HTLV-1 HBZ was amplified from a cDNA library generated from the HTLV-1^+ T-cell line C8166 by PCR and cloned into the expression vector pEF4/myc-His A (Invitrogen, Carlsbad, CA, USA). The expression vectors for c-Fos, Fra-1, Fra-2, c-Jun, JunB, JunD and Tax were described previously (Iwai *et al*., 2001). Cells (5×10^5) were transfected with 2 μg of reporter plasmid, 0.5 μg of expression plasmids for various transcription factors and 1 μg of pSV-β-galactosidase using DMRIE-C (Invitrogen). After 24–27 h, luciferase assays were performed using a Luciferase Assay kit (Promega). Luciferase activity was normalized by β-galactosidase activity that served as an internal control for transfection efficiency.

RT–PCR

RT–PCR was carried out as described previously (Yoshie *et al*., 2002). The primers used were as follows: +5′-AAGAA GAACAAGGCGGTGAAGATG-3′ and −5′-AGGCCCC TGCAGGTTTTGAAG-3′ for CCR4; +5′-TACTACCACTC ACCCGCAGACTC-3′ and −5′-CTTTTCCCTTCGGATTCT CCTTTT-3′ for c-Fos; +5′-TAGCAGCAGCTAAATGC AGGAAC-3′ and −5′-CCAGCTGAAGCCATCTTCCTT AG-3′ for FosB; +5′-CAGTGGATGGTACAGCCTCA TTT-3′ and −5′-GCCCAGATTTCTCATCTTCCAGT-3′ for Fra-1; +5′-CCAGCAGAAATTCCGGGTAGATA-3′ and −5′-TCTCCTCCTCTTCAGGAGACAGC-3′ for Fra-2; +5′-AAACAGAGCATGACCCTGAACCT-3′ and −5′-CTC CTGCTCATCTGTCACGTTCT-3′ for c-Jun; +5′-AAAAT GGAACAGCCCTTCTACCA-3′ and −5′-AGCCCTGACCA GAAAAGTAGCTG-3′ for JunB; +5′-AACACCCTTCT ACGGCGATGAG-3′ and −5′-GGGTAGAGGAACTGTG AGCTCGT-3′ for JunD; +5′-GAATTGGTGGACGGG CTATTATC-3′ and −5′-TAGCACTATGCTGTTTCGCCT TC-3′ for HBZ; +5′-CCGGCGCTGCTCTCATCCCGGT-3′ and −5′-GGCCGAACATAGTCCCCCAGAG-3′ for Tax; +5′-AAGGCATCCAGACCAGAAACCG-3′ and −5′-AGC ATCGAGCAGGGCTCTAACC-3′ for GATA-3; +5′-CAGT GACGAGGATGATGAGGACT-3′ and −5′-AACGTTTCG GACCGTATTTCTGT-3′ for c-Myb; +5′-ATTCCAGCTT CGGAACAAGAGAC-3′ and −5′-GTCCTTTTGATCAC TCCCACCTT-3′ for MDM2; +5′-CAAGAAGTTTCTAGG AAAGGCCGG-3′ and −5′-GATTGATCACACTAA GGTTGCATT-3′ for BCL-6 and +5′-GCCAAGGTCATCC ATGACAACTTTGG-3′ and −5′-GCCTGCTTCACCA CCTTCTTGATGTC-3′ for glyceraldehyde-3-phosphate dehydrogenase (GAPDH). The amplification conditions were denaturation at 94 °C for 30 s (5 min for the first cycle), annealing at 60 °C for 30 s and extension at 72 °C for 30 s (5 min for the last cycle) for 34 cycles for CCR4; 35 cycles for c-Fos, FosB, Fra-1, Fra-2, c-Jun, JunB, JunD, HBZ, Tax, c-Myb, BCL-6 and MDM2; 29 cycles for GATA-3 and 27 cycles for GAPDH. Amplification products were electrophoretically run on a 2% agarose gel and stained with ethidium bromide.

Quantitative real-time PCR was carried out using the TaqMan assay and a 7700 Sequence Detection System (Applied Biosystems, Foster City, CA, USA). The conditions for PCR were 50 °C for 2 min, 95 °C for 10 min and then 50 cycles of 95 °C for 15 s (denaturation) and 60 °C for 1 min (annealing extension). The primers and fluorogenic probes for CCR4 and 18S ribosomal RNA were obtained from a TaqMan kit (Applied Biosystems). Quantification of CCR4 expression was performed using the Sequence Detector System Software (Applied Biosystems).

NoShift transcription factor assay

Anti-c-Fos (sc-52), anti-FosB (sc-7203), anti-Fra-1 (sc-22794), anti-Fra-2 (sc-604), anti-c-Jun (sc-1694), anti-JunB (sc-73) and anti-JunD (sc-74) were purchased from Santa Cruz Biotechnology (Santa Cruz, CA, USA). Transcription factors bound to specific DNA sequences were identified using the NoShift Transcription Factor Assay Kit (EMD Biosciences, Madison, WI, USA). Nuclear extracts were prepared from human T-cell lines by using the NucBuster Protein Extraction Kit (EMD Biosciences). The oligonucleotides used were as follows (differences underlined): TGGGAAATGACTAAGAATCAT for the biotinylated probe and unlabeled competitor of the AP-1 site and TGGGAAATGTCAAAGAATCAT for the mutated AP-1 site.

ChIP assay

This assay was performed using a ChIP assay kit (Upstate Biotechnology, Lake Placid, NY, USA) following the manufacturer's instructions. In brief, cells (1×10^6) were cross-linked with 1% formaldehyde for 10 min at room temperature. The cell pellets were lysed with sodium dodecyl sulfate (SDS) lysis buffer and sonicated to shear DNA to a size range between 200 and 1000 bp. After centrifugation, the supernatant was diluted 10-fold in ChIP dilution buffer and incubated overnight at 4 °C with 4 μg of anti-Fra-2 (sc-604), anti-JunB (sc-73), anti-JunD (sc-74) or normal rabbit IgG (DAKO, Kyoto, Japan). Immunocomplexes were collected by adding protein A-agarose beads. The immune complexes were incubated at 65 °C for 4 h to reverse the protein/DNA cross-links. DNAs were then purified by phenol/chloroform extraction and used as templates for quantitative real-time PCR. The primers and

the fluorogenic probe for the AP-1 site of the CCR4 promoter were as follows: primers: +5′-GGTCTTGGGAAATGACT AAGAATCA-3′ and −5′-TCTCCCTCACCCAACTGTACT AAGT-3′; probe: 5′-TCTGCTTCCTACTTCTATCAAA AAACCCCACTTG-3′.

Immunological staining
Cells were spotted on a glass slide and fixed with 4% paraformaldehyde. Tissue sections were prepared from formalin-fixed and paraffin-embedded biopsy tissue samples and subjected to microwave irradiation for 5 min three times in Target Retrieval Solution (DAKO). Slides and tissue sections were incubated for 1 h at room temperature with anti-Fra-2 (sc-604), anti-JunB (sc-73), anti-JunD (sc-74) or mouse monoclonal anti-CCR4 (KM-2160; Kyowa Hakko, Tokyo, Japan). Normal rabbit IgG and control mouse IgG_1 (DAKO) were used as negative controls. After washing, the slides and tissue sections were incubated with biotin-labeled goat anti-rabbit IgG or biotin-labeled horse anti-mouse IgG followed by detection using the Vectastain ABC/HRP kit (Vector Laboratories, Burlingame, CA, USA). Finally, cells and sections were counterstained with Gill's hematoxylin (Polysciences, Warrington, PA, USA), dehydrated and mounted.

Transfection of siRNA
siRNAs for Fra-2 (SI00420455), JunB (SI03077445), JunD (SI00075985) and the negative control (1022064) were obtained from Qiagen (Hilden, Germany). Transfection experiments were performed using Amaxa Nucleofector (Amaxa, Cologne, Germany). Cells (1×10^6) were resuspended in 100 μl of Nucleofector solution (T solution for MOLT-4, HUT102 and ST1 and V solution for Jurkat) and transfected with 2.5 μg of siRNA using program O-17 for MOLT-4, HUT102 and ST1 and program S-18 for Jurkat. The transfection efficiency was ~95% as determined using fluorescent siRNA (Qiagen).

Cell proliferation assay
Cells were seeded in a 96-well plate at a density of 0.5×10^4 per well and cultured. The number of viable cells was determined every 24 h on a FACSCalibur system (Becton Dickinson, Mountain View, CA, USA) by gating out cells stained with propidium iodide. To prepare stable transfectants of Fra-2 and JunD, the coding regions of human Fra-2 and JunD were inserted into the pIRES2-EGFP vector (BD Biosciences, San Diego, CA, USA). Jurkat cells were transfected with the plasmids using DMRIE-C (Invitrogen). Stable transfectants expressing green fluorescence protein were sorted by flow cytometry using FACSVantage (Becton Dickinson).

Oligonucleotide microarray
Microarray analysis was performed as described previously (Igarashi *et al*., 2007) using the Affymetrix GeneChip HG-U133 Plus 2.0 array (Affymetrix, Santa Clara, CA, USA). In brief, the ATL-derived cell line ST1 was transfected with control siRNA or Fra-2 siRNA. Four independent transfections were performed for each group. After 48 h, total RNA samples were prepared and confirmed to be of good quality with the Agilent 2100 Bioanalyzer (Agilent Technologies, Waldbronn, Germany). All microarray data have been submitted to the Gene Expression Omnibus (GEO; http://www.ncbi.nlm.nih.gov/geo; accession no. GSE6379). The analysis was performed using the BRB Array Tools software version 3.3.0 (http://linus.nci.nih.gov/BRB-ArrayTools.html) developed by Richard Simon and Amy Peng.

Acknowledgements

We thank Namie Sakiyama for her excellent technical assistance. We also thank Dr Rich Simon and Dr Amy Peng for providing the BRB ArrayTools software. This work was supported in part by a Grant-in-Aid from the Ministry of Education, Culture, Sports and Technology, Japan; by Solution-Oriented Research for Science and Technology (SORST) from Japan Science and Technology Corporation and by High-Tech Research Center Project for Private Universities: matching fund subsidy from the Ministry of Education, Culture, Sports, Science and Technology of Japan, 2002–2009.

References

Basbous J, Arpin C, Gaudray G, Piechaczyk M, Devaux C, Mesnard JM. (2003). The HBZ factor of human T-cell leukemia virus type I dimerizes with transcription factors JunB and c-Jun and modulates their transcriptional activity. *J Biol Chem* **278**: 43620–43627.

Cesarman E, Chadburn A, Inghirami G, Gaidano G, Knowles DM. (1992). Structural and functional analysis of oncogenes and tumor suppressor genes in adult T-cell leukemia/lymphoma shows frequent p53 mutations. *Blood* **80**: 3205–3216.

Chang CC, Ye BH, Chaganti RS, Dalla-Favera R. (1996). BCL-6, a POZ/zinc-finger protein, is a sequence-specific transcriptional repressor. *Proc Natl Acad Sci USA* **93**: 6947–6952.

Chen F, Chen D, Rothenberg EV. (1999). Specific regulation of fos family transcription factors in thymocytes at two developmental checkpoints. *Int Immunol* **11**: 677–688.

Dang CV. (1999). c-Myc target genes involved in cell growth, apoptosis, and metabolism. *Mol Cell Biol* **19**: 1–11.

Eferl R, Wagner EF. (2003). AP-1: a double-edged sword in tumorigenesis. *Nat Rev Cancer* **3**: 859–868.

Ferenczi K, Fuhlbrigge RC, Pinkus J, Pinkus GS, Kupper TS. (2002). Increased CCR4 expression in cutaneous T cell lymphoma. *J Invest Dermatol* **119**: 1405–1410.

Galonek HL, Hardwick JM. (2006). Upgrading the BCL-2 Network. *Nat Cell Biol* **8**: 1317–1319.

Grassmann R, Aboud M, Jeang KT. (2005). Molecular mechanisms of cellular transformation by HTLV-1 Tax. *Oncogene* **24**: 5976–5985.

Hata T, Fujimoto T, Tsushima H, Murata K, Tsukasaki K, Atogami S *et al*. (1999). Multi-clonal expansion of unique human T-lymphotropic virus type-I-infected T cells with high growth potential in response to interleukin-2 in prodromal phase of adult T cell leukemia. *Leukemia* **13**: 215–221.

Hess JL, Bittner CB, Zeisig DT, Bach C, Fuchs U, Borkhardt A *et al*. (2006). c-Myb is an essential downstream target for homeobox-mediated transformation of hematopoietic cells. *Blood* **108**: 297–304.

Hori S, Nomura T, Sakaguchi S. (2003). Control of regulatory T cell development by the transcription factor Foxp3. *Science* **299**: 1057–1061.

Iellem A, Mariani M, Lang R, Recalde H, Panina-Bordignon P, Sinigaglia F *et al*. (2001). Unique chemotactic response profile and specific expression of chemokine receptors CCR4 and CCR8 by CD4(+)CD25(+) regulatory T cells. *J Exp Med* **194**: 847–853.

Igarashi T, Izumi H, Uchiumi T, Nishio K, Arao T, Tanabe M *et al*. (2007). Clock and ATF4 transcription system regulates drug resistance in human cancer cell lines. *Oncogene* **26**: 4749–4760.

Imai T, Nagira M, Takagi S, Kakizaki M, Nishimura M, Wang J *et al*. (1999). Selective recruitment of CCR4-bearing Th2 cells toward antigen-presenting cells by the CC chemokines thymus and

activation-regulated chemokine and macrophage-derived chemokine. *Int Immunol* **11**: 81–88.

Ishida T, Utsunomiya A, Iida S, Inagaki H, Takatsuka Y, Kusumoto S *et al.* (2003). Clinical significance of CCR4 expression in adult T-cell leukemia/lymphoma: its close association with skin involvement and unfavorable outcome. *Clin Cancer Res* **9**: 3625–3634.

Iwai K, Mori N, Oie M, Yamamoto N, Fujii M. (2001). Human T-cell leukemia virus type 1 tax protein activates transcription through AP-1 site by inducing DNA binding activity in T cells. *Virology* **279**: 38–46.

Jeang KT, Chiu R, Santos E, Kim SJ. (1991). Induction of the HTLV-I LTR by Jun occurs through the Tax-responsive 21-bp elements. *Virology* **181**: 218–227.

Jones D, O C, Kraus MD, Perez-Atayde AR, Shahsafaei A, Wu L *et al.* (2000). Expression pattern of T-cell-associated chemokine receptors and their chemokines correlates with specific subtypes of T-cell non-Hodgkin lymphoma. *Blood* **96**: 685–690.

Karreth F, Hoebertz A, Scheuch H, Eferl R, Wagner EF. (2004). The AP1 transcription factor Fra2 is required for efficient cartilage development. *Development* **131**: 5717–5725.

Karube K, Ohshima K, Tsuchiya T, Yamaguchi T, Kawano R, Suzumiya J *et al.* (2004). Expression of FoxP3, a key molecule in CD4CD25 regulatory T cells, in adult T-cell leukaemia/lymphoma cells. *Br J Haematol* **126**: 81–84.

Kerl K, Vonlanthen R, Nagy M, Bolzonello NJ, Gindre P, Hurwitz N *et al.* (2001). Alterations on the 5′ noncoding region of the BCL-6 gene are not correlated with BCL-6 protein expression in T cell non-Hodgkin lymphomas. *Lab Invest* **81**: 1693–1702.

Kim EJ, Hess S, Richardson SK, Newton S, Showe LC, Benoit BM *et al.* (2005). Immunopathogenesis and therapy of cutaneous T cell lymphoma. *J Clin Invest* **115**: 798–812.

Matsubara Y, Hori T, Morita R, Sakaguchi S, Uchiyama T. (2005). Phenotypic and functional relationship between adult T-cell leukemia cells and regulatory T cells. *Leukemia* **19**: 482–483.

Matsuoka M. (2003). Human T-cell leukemia virus type I and adult T-cell leukemia. *Oncogene* **22**: 5131–5140.

Migliazza A, Martinotti S, Chen W, Fusco C, Ye BH, Knowles DM *et al.* (1995). Frequent somatic hypermutation of the 5′ noncoding region of the BCL6 gene in B-cell lymphoma. *Proc Natl Acad Sci USA* **92**: 12520–12524.

Mori N, Fujii M, Ikeda S, Yamada Y, Tomonaga M, Ballard DW *et al.* (1999). Constitutive activation of NF-kappaB in primary adult T-cell leukemia cells. *Blood* **93**: 2360–2368.

Mori N, Fujii M, Iwai K, Ikeda S, Yamasaki Y, Hata T *et al.* (2000). Constitutive activation of transcription factor AP-1 in primary adult T-cell leukemia cells. *Blood* **95**: 3915–3921.

Nagakubo D, Jin Z, Hieshima K, Nakayama T, Shirakawa AK, Tanaka Y *et al.* (2007). Expression of CCR9 in HTLV-1$^+$ T cells and ATL cells expressing Tax. *Int J Cancer* **120**: 1591–1597.

Nagata K, Ohtani K, Nakamura M, Sugamura K. (1989). Activation of endogenous c-fos proto-oncogene expression by human T-cell leukemia virus type I-encoded p40tax protein in the human T-cell line, Jurkat. *J Virol* **63**: 3220–3226.

Oh IH, Reddy EP. (1999). The myb gene family in cell growth, differentiation and apoptosis. *Oncogene* **18**: 3017–3033.

Pasqualucci L, Bereschenko O, Niu H, Klein U, Basso K, Guglielmino R *et al.* (2003). Molecular pathogenesis of non-Hodgkin's lymphoma: the role of Bcl-6. *Leuk Lymphoma* **44**(Suppl 3): S5–S12.

Ramsay RG, Barton AL, Gonda TJ. (2003). Targeting c-Myb expression in human disease. *Expert Opin Ther Targets* **7**: 235–248.

Rayburn E, Zhang R, He J, Wang H. (2005). MDM2 and human malignancies: expression, clinical pathology, prognostic markers, and implications for chemotherapy. *Curr Cancer Drug Targets* **5**: 27–41.

Rengarajan J, Szabo SJ, Glimcher LH. (2000). Transcriptional regulation of Th1/Th2 polarization. *Immunol Today* **21**: 479–483.

Satou Y, Yasunaga J, Yoshida M, Matsuoka M. (2006). HTLV-I basic leucine zipper factor gene mRNA supports proliferation of adult T cell leukemia cells. *Proc Natl Acad Sci USA* **103**: 720–725.

Shaulian E, Karin M. (2002). AP-1 as a regulator of cell life and death. *Nat Cell Biol* **4**: E131–E136.

Shetzline SE, Rallapalli R, Dowd KJ, Zou S, Nakata Y, Swider CR *et al.* (2004). Neuromedin U: a Myb-regulated autocrine growth factor for human myeloid leukemias. *Blood* **104**: 1833–1840.

Shvarts A, Brummelkamp TR, Scheeren F, Koh E, Daley GQ, Spits H *et al.* (2002). A senescence rescue screen identifies BCL6 as an inhibitor of anti-proliferative p19(ARF)-p53 signaling. *Genes Dev* **16**: 681–686.

Thebault S, Basbous J, Hivin P, Devaux C, Mesnard JM. (2004). HBZ interacts with JunD and stimulates its transcriptional activity. *FEBS Lett* **562**: 165–170.

Vargas DA, Takahashi S, Ronai Z. (2003). Mdm2: a regulator of cell growth and death. *Adv Cancer Res* **89**: 1–34.

Yamada Y, Ohmoto Y, Hata T, Yamamura M, Murata K, Tsukasaki K *et al.* (1996). Features of the cytokines secreted by adult T cell leukemia (ATL) cells. *Leuk Lymphoma* **21**: 443–447.

Yamamoto N, Hinuma Y. (1985). Viral aetiology of adult T-cell leukaemia. *J Gen Virol* **66**: 1641–1660.

Ye BH, Lista F, Lo Coco F, Knowles DM, Offit K, Chaganti RS *et al.* (1993). Alterations of a zinc finger-encoding gene, BCL-6, in diffuse large-cell lymphoma. *Science* **262**: 747–750.

Yoshida M. (2001). Multiple viral strategies of HTLV-1 for dysregulation of cell growth control. *Annu Rev Immunol* **19**: 475–496.

Yoshie O, Fujisawa R, Nakayama T, Harasawa H, Tago H, Izawa D *et al.* (2002). Frequent expression of CCR4 in adult T-cell leukemia and human T-cell leukemia virus type 1-transformed T cells. *Blood* **99**: 1505–1511.

Yoshie O, Imai T, Nomiyama H. (2001). Chemokines in immunity. *Adv Immunol* **78**: 57–110.

N-Glycan fucosylation of epidermal growth factor receptor modulates receptor activity and sensitivity to epidermal growth factor receptor tyrosine kinase inhibitor

Kazuko Matsumoto,[1,3] Hideyuki Yokote,[1] Tokuzo Arao,[1] Mari Maegawa,[1] Kaoru Tanaka,[1] Yoshihiko Fujita,[1] Chikako Shimizu,[2] Toshiaki Hanafusa,[3] Yasuhiro Fujiwara[2] and Kazuto Nishio[1,4]

[1]Department of Genome Biology, Kinki University School of Medicine, 377-2 Ohno-Higashi, Osaka-Sayama, Osaka; [2]Medical Oncology, National Cancer Center Hospital, Tokyo; [3]First Department of Internal Medicine, Osaka Medical College, Osaka, Japan

(Received January 15, 2008/Revised April 16, 2008/Accepted April 16, 2008/Online publication July 29, 2008)

The glycosylation of cell surface proteins is important for cancer biology processes such as cellular proliferation or metastasis. α1,6-Fucosyltransferase (FUT8) transfers a fucose residue to *n*-linked oligosaccharides on glycoproteins. Herein, we study the effect of fucosylation on epidermal growth factor receptor (EGFR) activity and sensitivity to an EGFR-specific tyrosine kinase inhibitor (EGFR-TKI). The increased fucosylation of EGFR significantly promoted EGF-mediated cellular growth, and the decreased fucosylation by stable FUT8 knockdown weakened the growth response in HEK293 cells. The overexpression of FUT8 cells were more sensitive than the control cells to the EGFR-TKI gefitinib, and FUT8 knockdown decreased the sensitivity to gefitinib. Finally, to examine the effects in a human cancer cell line, we constructed stable FUT8 knockdown A549 cells, and found that these cells also decreased EGF-mediated cellular growth and were less sensitive than the control cells to gefitinib. In conclusion, we demonstrated that the modification of EGFR fucosylation affected EGF-mediated cellular growth and sensitivity to gefitinib. Our results provide a novel insight into how the glycosylation status of a receptor may affect the sensitivity of the cell to molecular target agents. (*Cancer Sci* 2008; 99: 1611–1617)

The glycosylation of cell surface proteins and lipids is modified during the course of differentiation, growth and aging, and various glycoprotein structures are important for biological functions.[1] Proteins and lipids are modified with *n*-linked oligosaccharides in the endoplasmic reticulum and Golgi apparatus. *n*-Linked oligosaccharides contribute to the folding and stability of glycoproteins.[2] Various glycosyltransferases have been cloned and are known to be involved in the formation of *n*-linked oligosaccharides.[3,4] Accumulating data has demonstrated that the modification of glycoforms can even change the phenotype of cells.[5]

Regarding the relationship between malignancy and *n*-linked oligosaccharides, glycoproteins on the cell surface are known to be altered in both quantity and quality during cancerous transformation.[6] Genes are known to determine the specific structures of oligosaccharides during regulated biological processes involved in cancer, such as metastasis.[7] For example, the knockout of *n*-acetylglucosaminyltransferaseV (GnT-V) has been reported to decrease metastasis in mice, indicating that GnT-V is deeply involved in cancer metastasis.[8]

Epidermal growth factor receptor (EGFR) is frequently expressed or highly expressed in lung cancer, ovarian cancer and many other solid tumors,[9–12] and a high expression level in tumor cells is closely related to a poor prognosis.[13,14] Therefore, EGFR is considered an important therapeutic target for the treatment of solid tumors. Tyrosine kinase inhibitors (TKI) that target EGFR, like gefitinib (IRESSA, ZD1839)[15–17] and erlotinib (Tarceva),[18] and the anti-EGFR antibody cetuximab (IMC-C225),[19] have been reported to exhibit potential antitumor effects in some solid tumors. Dramatic responses to gefitinib have been observed in non-small cell lung cancer (NSCLC) patients harboring activating mutations in the *EGFR* gene involving an exon 19 deletion or an L858R point mutation in exon 21.[20,21] However, the sensitivity of a cell to EGFR-TKI cannot be completely defined by these mutations because tumor response and disease stabilization with gefitinib have also been reported in some NSCLC patients with wild-type EGFR.[22,23] We have searched for predictive biomarkers that determine sensitivity to molecular targeted agents, including gefitinib.[24,25] Of additional interest, EGFR contains 11 potential *n*-glycosylation sites in its extracellular domain.[26] α1,6-Fucosyltransferase (FUT8) catalyzes the transfer of a fucose group to the innermost *n*-acetylglucosamine residue of complex *n*-glycans via α1,6-linkage in mammals. Wang *et al.* clearly demonstrated that the fucosylation of EGFR catalyzed by FUT8 regulates its receptor activity and signaling in murine cells.[27] However, whether receptor fucosylation affects the sensitivity of human cells to molecular target agents remains uncertain.

Accordingly, we studied the relationship between the fucosylation status of EGFR and sensitivity to gefitinib in HEK293 and a human NSCLC cell, A549.

Materials and Methods

Reagents. Gefitinib (IRESSA, ZD1839) was provided by AstraZeneca (Cheshire, UK).

Expression constructs and viral production. A full-length cDNA of FUT8, originating from a NSCLC cell line (A549),[28] was amplified using a reverse transcriptase polymerase chain reaction (RT-PCR). A High Fidelity RNA PCR Kit (TaKaRa, Otsu, Japan) was used for the RT-PCR, and the following primer set was synthesized: forward, GGA AGT GAG TTG AAA ATC TGA AA; reverse, ACT GAG TTT GGT CGT TTA TCT CT. The PCR products were amplified again using Pyrobest DNA polymerase (TaKaRa) and the following primer set: forward, GCG CTA GCA ATG CGG CCA TGG ACT GGT TC; reverse, CGT GGT ACC TTT CTC AGC CTC AGG ATA TGT. After confirming the sequence, FUT8 cDNA was transferred to

[4]To whom correspondence should be addressed. E-mail: knishio@med.kindai.ac.jp

doi: 10.1111/j.1349-7006.2008.00847.x

pcDNA3.1 (Invitrogen, Carlsbad, CA, USA) with a FLAG-tag at its C-terminus. *EGFR* cDNA with a myc-tag in pcDNA3.1 and FUT8 cDNA with a FLAG-tag were cut out and transferred into a pQCLIN retroviral vector (BD Biosciences Clontech, San Diego, CA, USA) together with enhanced green fluorescent protein (EGFP) followed by the internal ribosome entry site sequence (IRES) to monitor the expression of the inserts indirectly. A pVSV-G vector (Clontech, Palo Alt, CA, USA) for the constitution of the viral envelope, pGP vector (TAKARA Bio) and the pQCXIX constructs were co-transfected into the HEK293 cells using FuGene6 transfection reagent (Roche Diagnostics, Basel, Switzerland). Briefly, 80% confluent cells cultured in a 10-cm dish were transfected with 2 μg pVSV-G plus 6 μg pQCXIX vectors. Forty-eight hours after transfection, the culture medium was collected and the viral particles were concentrated by centrifugation at 15 000*g* for 3 h at 4°C. The viral pellet was then resuspended in fresh RPMI-1640 medium. The titer of the viral vector was calculated by counting the EGFP-positive cells that were infected by serial dilutions of a virus-containing medium and then determining the multiplicity of infection (MOI).

FUT8 knockdown by shRNA. We constructed a retroviral vector that stably expressed short hairpin RNA (shRNA) targeting human FUT8. The DNA sequences were designed as follows: forward, GAT CCG TCT CAG AAT TGG CGC TAT GCT GTG AAG CCA CAG ATG GGC ATA GCG CCA ATT CTG AGA CTT TTT TG; reverse, AAT TCA AAA AAG TCT CAG AAT TGG CGC TAT GCC CAT CTG TGG CTT CAC AGC ATA GCG CCA ATT CTG AGA CG. These oligonucleotides were annealed and inserted into an RNAi-Ready pSIREN-RetroQ-ZsGreen vector (Clontech). The viral particles were produced as described in the viral production section.

Cell culture and transfection. HEK293 (a human embryonic kidney cell line) was maintained in Dulbecco's modified Eagle's medium (DMEM) medium and A549 (an NSCLC cell line) was maintained in RPMI-1640 medium supplemented with 10% fetal bovine serum (FBS). HEK293/EGFR cells were transfected with retrovirus containing FUT8 gene or shRNA for FUT8 (shFUT8) or shRNA control construct and designed as 293/EGFR/FUT8, 293/EGFR/shFUT8 and 293/EGFR/control, respectively. A549 cells were transfected with either shFUT8 or shRNA control and designed as A549/shFUT8 and A549/control, respectively.

α1,6-Fucosyltransferase activity assay. Cells were lysed with a lysis buffer containing 1% Triton X, 20 mM Tris-HCl (pH 8.0) and 50 mM NaCl. The fluorescent substrate (GnGn-bi-Asn-PABA; Fig. 1a) was purchased from Peptide Institute (Osaka, Japan). The standard mixture for measuring FUT8 activity contained 50 μM substrate, 200 mM MES (pH 7.0), 1% Triton X, 500 μM GDP-Fucose and the cell lysate in a final volume of 50 μL. The reaction mixture was incubated at 37°C for 6 h, and the reaction was stopped by heating at 100°C for 1 min. The sample was then centrifuged at 15 000*g* for 10 min and the supernatant (10 μL) was used for analysis. The product was separated using high-performance liquid chromatography (HPLC) with a TSK-gel ODS-80TM column (4.6 mm × 150 mm). Elution was performed at 55°C with a 20 mM acetate buffer, pH 4.0, containing 0.1% butanol. The fluorescence of the column elute was detected using a fluorescence photometer (Hitachi Fluorescence Spectrophotometer 650–10LC). The excitation and emission wavelengths were observed at 320 and 400 nm, respectively.[29]

Immunoprecipitation and immunoblotting. A549 cells were lysed with a lysis buffer containing 1% Triton X, 20 mM Tris-HCl (pH 7.0), 5 mM ethylenediaminetetraacetic acid (EDTA), 50 mM NaCl, 10 mM Na pyrophosphate, 50 mM NaF, 1 mM Na orthovanadate, and a Complete Mini protease inhibitor mix (Roche Diagnostics). The cell lysate (1 mg) was immunoprecipitated by incubation with anti-EGFR antibody (Upstate Biotechnology, Lake Placid, NY, USA) overnight, followed by further incubation with protein-G agarose (Santa Cruz Biotechnology, Santa Cruz, CA, USA) for 1 h and washed with lysis buffer three times. Whole cell lysates and immunoprecipitated samples were separated using sodium dodecylsulfate polyacrylamide gel electrophoresis (SDS-PAGE) and blotted on a polyvinylidene fluoride (PVDF) membrane. The membranes were blocked with 3% bovine serum albumin (BSA) in Tris-buffered saline with 0.05% Tween-20 (TBST) and then probed with monoclonal anti-EGFR antibody (Upstate Biotechnology), monoclonal phospho-tyrosine antibody, p44/42 MAP kinase antibody or phospho-p44/42 MAP kinase antibody (Cell Signaling, Beverly, MA, USA), followed by incubation with a monoclonal or polyclonal HRP-conjugated secondary antibody (Cell Signaling). An enhanced chemiluminescence detection system (GE Healthcare, Buckinghamshire, UK) was then used for visualization. Images were visualized by LAS-3000 (Fujifilm, Tokyo, Japan) and the data were quantified by automated densitometry using Multigauge ver. 3.0 (Fujifilm).

Lectin blotting. Whole cell lysates and immunoprecipitated samples were separated using SDS-PAGE and blotted on a PVDF membrane. The membrane was blocked with 5% BSA in TBST for 1 h at room temperature. The membrane was probed with biotinylated aleuria aurantia lectin (AAL, Seikagaku, Tokyo, Japan) for 1 h at room temperature, washed, and treated using the Vectastain ABC kit (Vector Laboratories, Burlingame, CA, USA) as a second antibody.

Cell proliferation assay. To evaluate the growth response to EGF stimulation, we used the tetrazolium dye (3,4,5-dimethyl-2H-tetrazolium bromide, MTT) assay. The cells were seeded at a density of 0.5–1.5 × 10^3 cells/well in 96-well plates under a serum-reduced condition (HEK293 cells, 4% FBS; A549 cells, 2% FBS). Twenty-four hours later, the cells were stimulated with EGF (R&D Systems, Minneapolis, MN, USA) at 20 ng/mL. After 48–72 h of incubation at 37°C, the MTT solution was added to each well and the plates were incubated for 3 h at 37°C. After centrifuging the plates at 400*g* for 5 min, the medium was discarded from each well, and 200 μL of dimethylsulfoxide was added to each well. The optical density was measured at 570 nm. For the growth curve experiments, the cells were seeded at a density of 2 × 10^3 cells/well in 96-well plates in the presence of 10% FBS or under the serum-reduced condition in the presence of 20 ng/mL of EGF. Cell proliferation was estimated by measuring the absorbance at 570 nm at 24 h intervals up to 72 h.

Growth inhibitory assay. To evaluate the growth inhibition in the presence of various concentrations of gefitinib, we used the MTT assay. The cells were seeded at a density of 1.5 or 2 × 10^3 cells/well in 96-well plates in the presence of 10% FBS or under the serum-reduced condition in the presence of 20 ng/mL of EGF. Twenty-four hours later, gefitinib was added and the incubation was continued further for 72 h at 37°C. The assay was conducted in triplicate.

Soft agar assay for colony formation. To confirm the data obtained from the growth inhibitory assay, we performed colony assays of A549 cells. Five hundred cells in 0.35% agar in DMEM containing 10% FBS and each concentration of EGF or gefitinib were seeded onto 6-well plates on an underlayer of 0.5% agar containing DMEM. The plates were incubated at 37°C for 14 days, and then the colonies were stained by crystal violet and counted under a microscope. The colony assay was performed in triplicate.

Statistical analysis. All statistical calculations were performed using a Student's *t*-test by StatView ver. 5 software (SAS Institute, Cary, NC, USA). $P < 0.05$ was considered significant.

Result

Establishment of FUT8 overexpression and knockdown cells. To examine whether an increase or decrease in the fucosylation of

doi: 10.1111/j.1349-7006.2008.00847.x

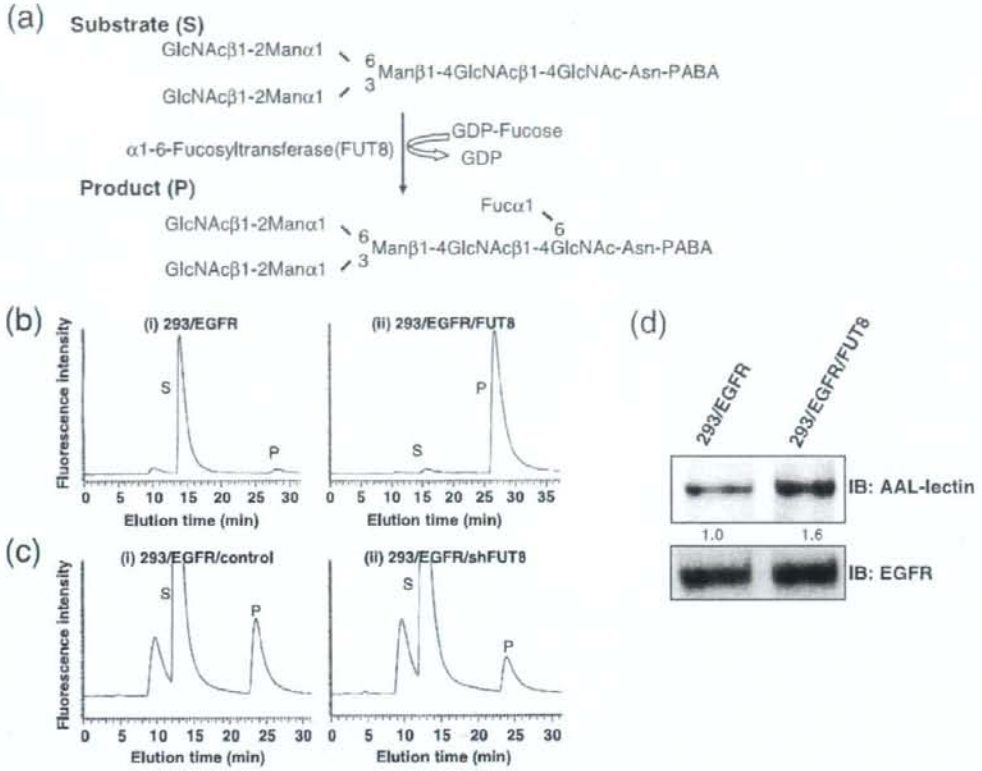

Fig. 1. α1,6-Fucosyltransferase (FUT8) enzyme activity of HEK293 cells. (a) Schema of FUT8 reaction pathway. Asn, asparagine; Fuc, Fucose; Man, mannose; PABA, 4-(2-pyridylamino) butylamine. (b) Analysis of FUT8 activity in cells overexpressing FUT8. FUT8 activity was measured using high-performance liquid chromatography. (i) 293/EGFR; (ii) 293/EGFR/FUT8. P, product; S, substrate. (c) Analysis of FUT8 activity in FUT8 knockdown cells. (i) 293/EGFR/control; (ii) 293/EGFR/shFUT8. (d) Effect of FUT8 overexpression on epidermal growth factor receptor (EGFR) fucosylation. The cell lysate from 293/EGFR or 293/EGFR/FUT8 cells was subjected to sodium dodecylsulfate polyacrylamide gel electrophoresis followed by lectin blotting using biotinylated *Aleuria aurantia* lectin (AAL). IB, immunoblot.

EGFR affected EGF-mediated cellular growth and sensitivity to gefitinib, we transfected EGFR and FUT8 retrovirally. We also constructed 293/EGFR/shFUT8 cells by the stable knockdown of intrinsic FUT8. FUT8 enzyme activity was measured by reverse-phase HPLC using a fluorescent substrate (GnGn-bi-Asn-PABA; Fig. 1a). FUT8 activity was 25-times higher in 293/EGFR/FUT8 cells than in 293/EGFR (44.1 U/L and 1.8 U/L, respectively; Fig. 1b). On the other hand, the activity in 293/EGFR/shFUT8 cells was 43% of that in 293/EGFR/control cells (Fig. 1c). We next compared fucosylated EGFR between 293/EGFR and 293/EGFR/FUT8 cells using lectin blotting with *Aleuria aurantia* lectin, which recognizes core fucosylation on *n*-glycans. The fucosylation of EGFR was increased in 293/EGFR/FUT8 cells, compared with that in 293/EGFR cells (Fig. 1d). These findings indicated that the overexpression or knockdown of FUT8 was functional and FUT8 regulated the fucosylation of EGFR, as expected.

EGFR fucosylation regulates EGF-mediated cellular growth in HEK293 and A549 cells. We next examined whether EGFR fucosylation affected the cellular growth in response to EGF ligand stimulation. Overexpression of FUT8 was associated with a significant increase, by approximately 20%, of the cellular growth in response to EGF stimulation ($P < 0.05$; Fig. 2a). In growth curve experiments, the proliferative activity of 293/EGFR/FUT8 cells was slightly increased as compared with that of 293/EGFR cells under normal conditions of culture in the presence of 10% FBS (Fig. 2b). The doubling times of 293/EGFR/FUT8 and 293/EGFR cells were 27.5 and 28.5 h, respectively. However, remarkable increase of the proliferative activity of 293/EGFR/FUT8 cells was observed as compared with that of the 293/EGFR cells in the presence of EGF stimulation ($P < 0.05$; Fig. 2c); the doubling times under this condition were 23.9 and 25.4 h, respectively. Next, FUT8 knockdown significantly decreased, by approximately 20%, the cellular growth in response to EGF stimulation ($P < 0.05$; Fig. 2d). In growth curve experiments, there was no difference in the proliferative activity between 293/EGFR/shFUT8 cells and 293/EGFR/control cells under normal conditions of culture (Fig. 2e), but significant decrease of the proliferative activity of 293/EGFR/shFUT8 cells was found as compared with that of the 293/EGFR/control cells in the presence of EGF stimulation ($P < 0.05$; Fig. 2f); the doubling times of the 293/EGFR/shFUT8 and 293/EGFR/control cells under this condition were 28.8 and 27.3 h, respectively. These findings suggest that the level of EGFR fucosylation regulated the cellular growth in response to EGF. To study whether the same phenomenon

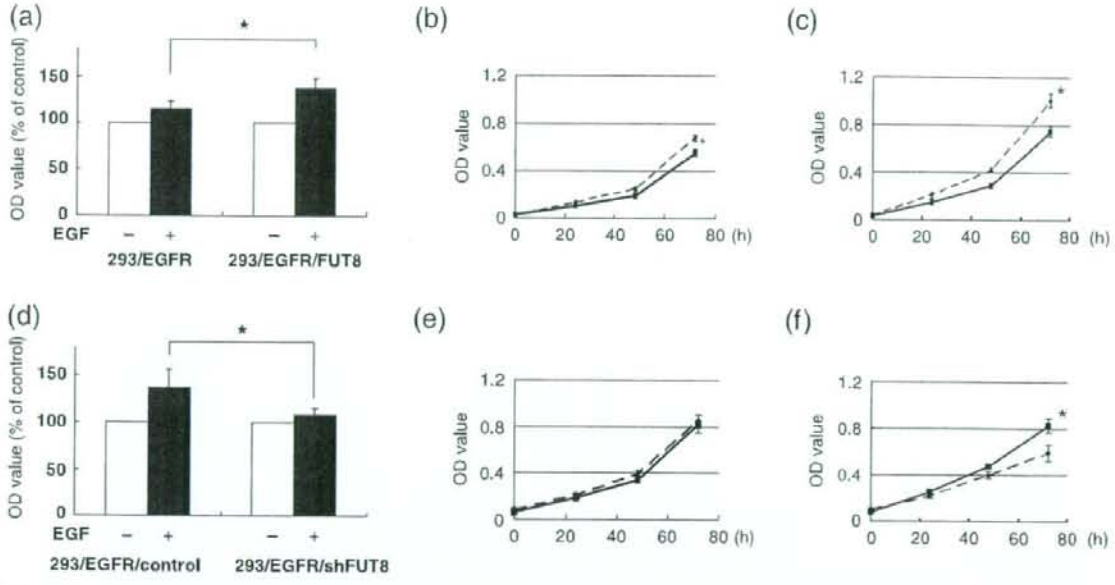

Fig. 2. Cellular growth response to epidermal growth factor (EGF) stimulation in HEK293 cells. (a) The 293/EGFR and 293/EGFR/FUT8 cells were seeded (1.5×10^3 cells/well) in 96-well plates under a serum-reduced condition and stimulated with 20 ng/mL of EGF and further incubated for 48 h at 37°C. (□), EGF (–); (■), EGF (+). (b) Growth curve experiments in the 293/EGFR (solid line) and 293/EGFR/FUT8 (dotted line) cells. The cells were cultured under a 10% fetal bovine serum (FBS) condition. (c) The 293/EGFR (solid line) and 293/EGFR/FUT8 (dotted line) cells were cultured under the presence of 20 ng/mL of EGF to a serum-reduced condition. (d) The 293/EGFR/control and 293/EGFR/shFUT8 cells were seeded (1.5×10^3 cells/well) in 96-well plates under a serum-reduced condition and stimulated with 20 ng/mL of EGF and incubated for 72 h at 37°C. (□), EGF (–); (■), EGF (+). (e) Growth curve experiments in the 293/EGFR/control (solid line) and 293/EGFR/shFUT8 (dotted line) cells. The cells were cultured under a 10% FBS condition. (f) The 293/EGFR/control (solid line) and 293/EGFR/shFUT8 (dotted line) cells were cultured under the presence of 20 ng/mL of EGF to a serum-reduced condition. OD value, 570 nm. *$P < 0.05$; scale lines, standard deviation (SD).

occurs in human cancer cells, we constructed A549/shFUT8, in which FUT8 was stably knocked down, and examined the relationship between the fucosylation level of EGFR and the response to EGF ligand stimulation. No FUT8 catalytic activity was detected by FUT8 knockdown in the A549 cells (Fig. 3a). A lectin blot analysis demonstrated that the fucosylation of EGFR was decreased in A549/shFUT8 cells, while the expression level of EGFR was similar in the control cells (Fig. 3b). We examined whether this reduction in EGFR fucosylation affected the EGF-mediated growth response. We found that A549/shFUT8 cells had significantly decreased EGF-mediated cellular growth by approximately 20%, compared with control cells ($P < 0.05$; Fig. 3c) by the MTT assay. In the growth curve experiments, a slight decrease of the proliferative activity of the A549/shFUT8 cells was observed as compared with that of the A549/control cells under normal conditions of culture in the presence of 10% FBS (Fig. 3d); the doubling times of the A549/shFUT8 and A549/control cells were 23.1 and 22.7 h, respectively. However, the A549/shFUT8 cells showed marked decrease of proliferative activity as compared with A549/control cells in the presence of EGF stimulation ($P < 0.05$, Fig. 3e); the doubling times of the A549/shFUT8 and A549/control cells were 22.2 and 20.8 h, respectively. These results suggest that the level of EGFR fucosylation regulated the cellular growth in response to EGF even in human cancer cells.

Modification of EGFR fucosylation affects cell sensitivity to gefitinib. We then examined whether an increase or decrease in EGFR fucosylation affected the sensitivity of HEK293 cells to gefitinib. Overexpression of FUT8 significantly enhanced the cellular sensitivity to gefitinib as compared with that of the control cells in the presence of EGF under a serum-reduced condition; the IC_{50} values of the drug for these cells were 3.5 ± 0.1 and 5.6 ± 0.3, respectively ($P < 0.05$; Fig. 4a). However, no significant difference in the IC_{50} values of the drug was noted between the two types of cells under normal culture conditions in the presence of 10% FBS (Fig. 4b). In addition, FUT8 knockdown significantly decreased the cellular sensitivity to gefitinib as compared with that of the control cells in the presence of EGF under the serum-reduced condition; the IC_{50} values of the drug for these cells were 7.3 ± 0.4 and 4.4 ± 1.0, respectively ($P < 0.05$; Fig. 4c). On the other hand, no significant difference in the IC_{50} values of the drug were noted among the cells when they were cultured under normal conditions (Fig. 4d). These results suggest that EGFR fucosylation modulates the cellular sensitivity to gefitinib.

We also examined the sensitivity of A549 cells to gefitinib. FUT8 knockdown significantly decreased the sensitivity of the A549 cells to gefitinib in the presence of 20 ng/mL of EGF under the serum-reduced condition; the IC_{50} values of the A549/shFUT8 and A549/control cells were 3.1 ± 0.3 and 1.3 ± 0.2, respectively ($P < 0.05$; Fig. 5a). However, no significant difference in the IC_{50} values were noted among the cells when they were cultured under normal conditions, similar to the observations for HEK293 cells (Fig. 5b). These results suggest that the EGFR fucosylation level affected the sensitivity of human cancer cells to gefitinib. To confirm the data obtained from the growth inhibitory assay, we performed colony assays with the A549 cells. Colony formation of A549/control, but not of the A549/shFUT8 cells, was significantly inhibited by 1 μM gefitinib ($P < 0.05$; Fig. 5c).

doi: 10.1111/j.1349-7006.2008.00847.x

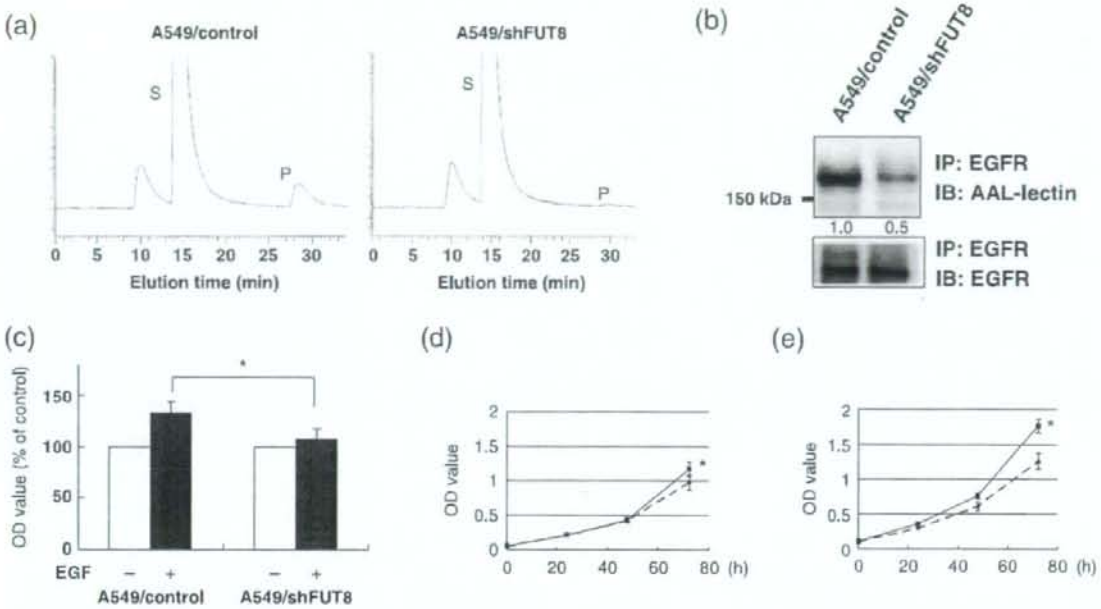

Fig. 3. α1,6-Fucosyltransferase (FUT8) knockdown weakened growth response to epidermal growth factor (EGF) stimulation in A549 cells. (a) FUT8 activity was analyzed using high-performance liquid chromatography. P, product; S, substrate. (b) Effect of FUT8 knockdown on EGF receptor (EGFR) fucosylation in A549 cells. The cell lysate was immunoprecipitated using anti-EGFR antibody, and the sample was separated using sodium dodecylsulfate polyacrylamide gel electrophoresis followed by blotting biotinylated *Aleuria aurantia* lectin (AAL) or monoclonal anti-EGFR antibody. IB, immunoblot; IP, immunoprecipitate. (c) The cells were seeded (0.5×10^3 cells/well) in 96-well plates under a serum-reduced condition. Twenty-four hours later, the cells were stimulated with 20 ng/mL of EGF and further incubated for 48 h. (□), EGF (–); (■), EGF (+). (d) Growth curve experiments in the A549/control (solid line) and A549/shFUT8 (dotted line) cells. The cells were cultured under a 10% fetal bovine serum condition. (e) The A549/control (solid line) and A549/shFUT8 (dotted line) cells were cultured under the presence of 20 ng/mL of EGF to a serum-reduced condition. OD value, 570 nm. $^*P < 0.05$; scale lines, standard deviation.

Fucosylation status of EGFR regulates EGFR signaling. We examined the effect of FUT8 knockdown on the phosphorylation levels of EGFR and the EGFR-mediated intracellular signaling pathway in A549 cells. FUT8 knockdown decreased the phosphorylation levels of EGFR in the presence of EGF stimulation (Fig. 5d). FUT8 knockdown also decreased the EGF-mediated phosphorylation of mitogen-activated protein kinase in the presence of 0.2 and 2 ng/mL of EGF (Fig. 5e). These results suggest that low EGFR fucosylation levels decrease the EGFR-mediated intracellular signaling pathway's response to EGF stimulation.

Discussion

The purpose of this study was to investigate whether the modification of EGFR fucosylation affected EGF-mediated cellular growth and cell sensitivity to gefitinib. We found that the increase in EGFR fucosylation resulting from FUT8 overexpression enhanced the response to EGF stimulation and the sensitivity of the cells to gefitinib. A decrease in EGFR fucosylation resulting from FUT8 knockdown weakened the EGF-mediated cellular growth response and cell sensitivity.

Two possible mechanisms may explain how EGFR fucosylation affects the EGF-mediated growth response. First, the binding affinity of EGFR to the EGF ligand might be affected by the modified fucosylation of the receptor. *n*-Acetylglucosaminyltransferase III (GnT III) is known to catalyze the addition of *n*-acetylglucosamine in β1-4 linkage to the β-linked mannose of the trimannosyl core of *n*-linked oligosaccharides to produce a bisecting GlcNac residue. Rebbaa *et al.* reported that the overexpression of GnT III in glioma cells modifies the glycosylation of its receptor, resulting in a decrease in EGF binding and EGFR autophosphorylation;[30] this finding suggests that the carbohydrate structure at the extracellular domain of EGFR affects the binding affinity with its ligand and the receptor activity. This evidence supports this first possible mechanism. Another possibility is that the ability of the receptor to form dimers might be affected by the glycosylation of the receptor. Tsuda *et al.* reported that a specific *n*-glycosylation mutant of domain III of EGFR leads to ligand-independent dimerization and phosphorylation, resulting in the spontaneous activation of the receptor.[31] These findings indicate that *n*-linked oligosaccharides in extracellular domain III of EGFR play a crucial role in receptor dimerization, independent of ligand binding. The type III EGFR (EGFRvIII), which lacks exons 2–7 in the extracellular domain, is constitutively phosphorylated independently of EGF-ligand stimulation. Fernandes *et al.* demonstrated that the receptor–receptor self association is highly dependent on a conformation induced by *n*-linked glycosylation, suggesting that *n*-linked oligosaccharides play an important role in this autodimerization.[32]

Regarding fucosylation, Wang *et al.* reported that EGF decreased EGF binding to EGFR in Fut8 knockout mice, resulting in a higher responsiveness of the receptor to its ligand.[27] Many studies have reported that the *mutant* EGFR (i.e. 15-base deletion or L858R) signaling is constitutively active without ligand condition. Thus, we speculated that wild-type EGFR

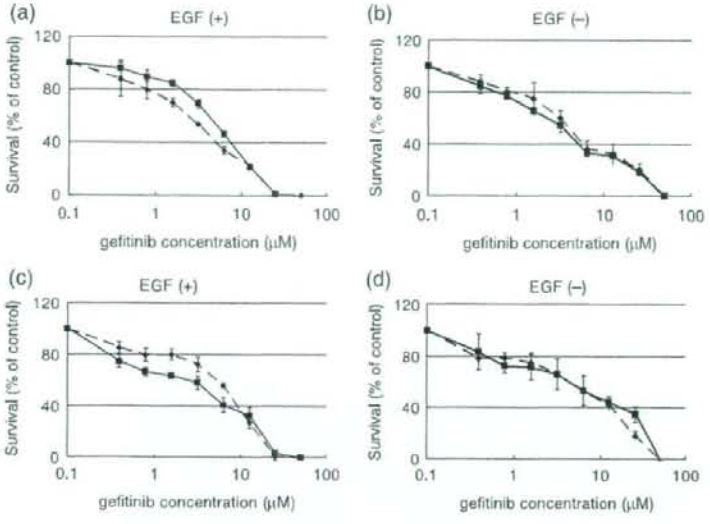

Fig. 4. Sensitivity of HEK293 cells to gefitinib. The cells were seeded at a density of 2×10^3 cells/well in 96-well plates. Twenty-four hours later, the cells were exposed to gefitinib and were then incubated for 72 h at 37°C. The cell growth was quantitated using an 3,4,5-dimethyl-2H-tetrazolium bromide (MTT) assay. (a) 293/EGFR (solid line) and 293/EGFR/FUT8 (dotted line) were cultured under the presence of 20 ng/mL of EGF to a serum-reduced condition. (b) 293/EGFR (solid line) and 293/EGFR/FUT8 (dotted line) were cultured under a 10% fetal bovine serum (FBS) condition. (c) 293/EGFR/control cells (solid line) and 293/EGFR/shFUT8 cells (dotted line) were cultured under the presence of 20 ng/mL of EGF to a serum-reduced condition. (d) 293/EGFR/control cells (solid line) and 293/EGFR/shFUT8 cells (dotted line) were cultured under a 10% FBS condition. Scale lines, standard deviation.

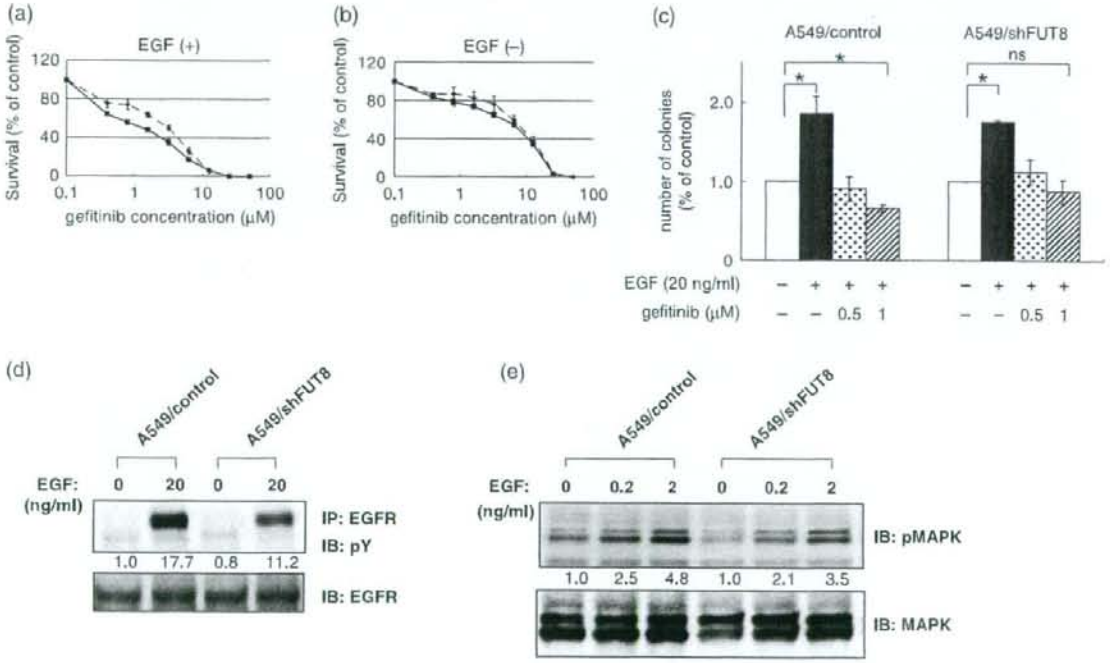

Fig. 5. α1,6-Fucosyltransferase (FUT8) knockdown decreased the sensitivity of A549 cells to gefitinib, epidermal growth factor receptor (EGFR) phosphorylation and EGFR-mediated intracellular signaling. (a) A549/control cells (solid line) and A549/shFUT8 cells (dotted line) were seeded at a density of 1.5×10^3 cells/well in 96-well plates. Twenty-four hours later, the cells were exposed to gefitinib and were then incubated for 72 h at 37°C. The cells were cultured under the presence of 20 ng/mL of EGF to a serum-reduced condition. (b) A549/control cells (solid line) and A549/shFUT8 cells (dotted line) were cultured under a 10% fetal bovine serum condition. Scale lines, standard deviation (SD). (c) Colony assay in A549/control cells and A549/shFUT8 cells. The cells were cultured for 14 days under the presence or absence of EGF or gefitinib. $^*P < 0.05$; scale lines, SD. (d) A549 cells were cultured under a serum-free condition for 6 h, and the cells were stimulated with 20 ng/mL of EGF for 10 min. The cell lysate was immunoprecipitated using anti-EGFR antibody and immunoblotted using antiphospho-tyrosine antibody (pY). (e) A549 cells were stimulated with 0.2 ng/mL or 2 ng/mL EGF for 10 min. The cell lysate was separated using sodium dodecylsulfate polyacrylamide gel electrophoresis and then immunoblotted using antiphospho p44/42 mitogen-activated protein kinase (pMAPK) antibody and antip44/42 MAPK (MAPK) antibody. IB, immunoblot; IP, immunoprecipitate.

doi: 10.1111/j.1349-7006.2008.00847.x

might be suitable for a study of the effects of fucosylation. Our results also demonstrate that modifications of EGFR fucosylation through the overexpression or knockdown of FUT8 alter EGF-mediated cellular growth responses in both HEK293 and A549 cells.

Epidermal growth factor receptor is overexpressed in various human tumors, and the overexpression of EGFR is associated with a poor prognosis.[33] Many researchers have studied the biological and clinical significance of *EGFR* mutations, including exon 19 deletions and the L858R point mutation in exon 21, which behave like constitutively-active receptors.[34-36] Patients with constitutively-active mutants of *EGFR* are more sensitive to gefitinib. However, some patients respond to EGFR-TKI even though they do not carry such *EGFR* mutations;[22,23] suggesting the presence of one or more undefined factors that affects sensitivity to gefitinib in addition to *EGFR* mutations. Although the impact on sensitivity to gefitinib is smaller than that of EGFR mutations, we have shown that modifications in wild-type EGFR fucosylation also affect sensitivity to gefitinib. Our findings raise the possibility that the status of EGFR fucosylation may be another determinant of sensitivity to gefitinib.

In conclusion, we have demonstrated that the fucosylation level of EGFR, which was regulated by FUT8, modifies EGF-mediated cellular growth and affects sensitivity to gefitinib.

Acknowledgments

This work was supported by funds for the Third-Term Comprehensive 10-Year Strategy for Cancer Control and for Health and Labor Scientific Research Grants, Research on Advanced Medical Technology H17-Pharmaco-006. K. M is the recipient of a Research Resident Fellowship from the Foundation of Promotion of Cancer Research in Japan.

References

1 Hakomori Si SI. Inaugural Article: The glycosynapse. *Proc Natl Acad Sci USA* 2002; **99**: 225–32.
2 Helenius A, Aebi M. Intracellular functions of N-linked glycans. *Science* 2001; **291**: 2364–9.
3 Sato T, Furukawa K, Bakker H, Van den Eijnden DH, Van Die I. Molecular cloning of a human cDNA encoding beta-1,4-galactosyltransferase with 37% identity to mammalian UDP-Gal: GlcNAc beta-1,4-galactosyltransferase. *Proc Natl Acad Sci USA* 1998; **95**: 472–7.
4 Almeida R, Amado M, David L *et al.* A family of human beta4-galactosyltransferases. Cloning and expression of two novel UDP-galactose: beta-n-acetylglucosamine beta1, 4-galactosyltransferases, beta4Gal-T2 and beta4Gal-T3. *J Biol Chem* 1997; **272**: 31 979–91.
5 Coetzee T, Fujita N, Dupree J *et al.* Myelination in the absence of galactocerebroside and sulfatide: normal structure with abnormal function and regional instability. *Cell* 1996; **86**: 209–19.
6 Dennis JW. Asn-linked oligosaccharide processing and malignant potential. *Cancer Surv* 1988; **7**: 573–95.
7 Dennis JW, Laferte S, Waghorne C, Breitman ML, Kerbel RS. Beta 1-6 branching of Asn-linked oligosaccharides is directly associated with metastasis. *Science* 1987; **236**: 582–5.
8 Granovsky M, Fata J, Pawling J, Muller WJ, Khokha R, Dennis JW. Suppression of tumor growth and metastasis in Mgat5-deficient mice. *Nat Med* 2000; **6**: 306–12.
9 Ang KK, Berkey BA, Tu X *et al.* Impact of epidermal growth factor receptor expression on survival and pattern of relapse in patients with advanced head and neck carcinoma. *Cancer Res* 2002; **62**: 7350–6.
10 Rusch V, Klimstra D, Venkatraman E, Pisters PW, Langenfeld J, Dmitrovsky E. Overexpression of the epidermal growth factor receptor and its ligand transforming growth factor alpha is frequent in resectable non-small cell lung cancer but does not predict tumor progression. *Clin Cancer Res* 1997; **3**: 515–22.
11 Watanabe K, Tachibana O, Sata K, Yonekawa Y, Kleihues P, Ohgaki H. Overexpression of the EGF receptor and p53 mutations are mutually exclusive in the evolution of primary and secondary glioblastomas. *Brain Pathol* 1996; **6**: 217–23; discussion 23–4.
12 Lipponen P, Eskelinen M. Expression of epidermal growth factor receptor in bladder cancer as related to established prognostic factors, oncoprotein (c-erbB-2, p53) expression and long-term prognosis. *Br J Cancer* 1994; **69**: 1120–5.
13 Khorana AA, Ryan CK, Cox C, Eberly S, Sahasrabudhe DM. Vascular endothelial growth factor, CD68, and epidermal growth factor receptor expression and survival in patients with Stage II and Stage III colon carcinoma: a role for the host response in prognosis. *Cancer* 2003; **97**: 960–8.
14 Magne N, Pivot X, Bensadoun RJ *et al.* The relationship of epidermal growth factor receptor levels to the prognosis of unresectable pharyngeal cancer patients treated by chemo-radiotherapy. *Eur J Cancer* 2001; **37**: 2169–77.
15 Koizumi F, Kanzawa F, Ueda Y *et al.* Synergistic interaction between the EGFR tyrosine kinase inhibitor gefitinib ('Iressa') and the DNA topoisomerase I inhibitor CPT-11 (irinotecan) in human colorectal cancer cells. *Int J Cancer* 2004; **108**: 464–72.
16 Naruse I, Ohmori T, Ao Y *et al.* Antitumor activity of the selective epidermal growth factor receptor-tyrosine kinase inhibitor (EGFR-TKI) Iressa (ZD1839) in an EGFR-expressing multidrug-resistant cell line in vitro and in vivo. *Int J Cancer* 2002; **98**: 310–15.
17 Fukuoka M, Yano S, Giaccone G *et al.* Multi-institutional randomized phase II trial of gefitinib for previously treated patients with advanced non-small-cell lung cancer. *J Clin Oncol* 2003; **21**: 2237–46.
18 Sandler A. Clinical experience with the HER1/EGFR tyrosine kinase inhibitor erlotinib. *Oncology (Huntingt)* 2003; **17**: 17–22.
19 Herbst RS, Hong WK. IMC-C225, an anti-epidermal growth factor receptor monoclonal antibody for treatment of head and neck cancer. *Semin Oncol* 2002; **29**: 18–30.
20 Lynch TJ, Bell DW, Sordella R *et al.* Activating mutations in the epidermal growth factor receptor underlying responsiveness of non-small-cell lung cancer to gefitinib. *N Engl J Med* 2004; **350**: 2129–39.
21 Paez JG, Janne PA, Lee JC *et al.* EGFR mutations in lung cancer: correlation with clinical response to gefitinib therapy. *Science* 2004; **304**: 1497–500.
22 Han SW, Kim TY, Hwang PG *et al.* Predictive and prognostic impact of epidermal growth factor receptor mutation in non-small-cell lung cancer patients treated with gefitinib. *J Clin Oncol* 2005; **23**: 2493–501.
23 Takano T, Ohe Y, Sakamoto H *et al.* Epidermal growth factor receptor gene mutations and increased copy numbers predict gefitinib sensitivity in patients with recurrent non-small-cell lung cancer. *J Clin Oncol* 2005; **23**: 6829–37.
24 Kimura H, Kasahara K, Kawaishi M *et al.* Detection of epidermal growth factor receptor mutations in serum as a predictor of the response to gefitinib in patients with non-small-cell lung cancer. *Clin Cancer Res* 2006; **12**: 3915–21.
25 Sakai K, Yokote H, Murakami-Murofushi K, Tamura T, Saijo N, Nishio K. In-frame deletion in the EGF receptor alters kinase inhibition by gefitinib. *Biochem J* 2006; **397**: 537–43.
26 Whitson KB, Whitson SR, Red-Brewer ML *et al.* Functional effects of glycosylation at Asn-579 of the epidermal growth factor receptor. *Biochemistry* 2005; **44**: 14 920–31.
27 Wang X, Gu J, Ihara H, Miyoshi E, Honke K, Taniguchi N. Core fucosylation regulates epidermal growth factor receptor-mediated intracellular signaling. *J Biol Chem* 2006; **281**: 2572–7.
28 Fukuoka K, Nishio K, Fukumoto H *et al.* Ectopic p16 (ink4) expression enhances CPT-11-induced apoptosis through increased delay in S-phase progression in human non-small-cell-lung-cancer cells. *Int J Cancer* 2000; **86**: 197–203.
29 Uozumi N, Teshima T, Yamamoto T *et al.* A fluorescent assay method for GDP-L-Fuc: N-acetyl-beta-D-glucosaminide alpha 1-6fucosyltransferase activity, involving high performance liquid chromatography. *J Biochem (Tokyo)* 1996; **120**: 385–92.
30 Rebbaa A, Yamamoto H, Saito T *et al.* Gene transfection-mediated overexpression of beta1,4-N-acetylglucosamine bisecting oligosaccharides in glioma cell line U373 MG inhibits epidermal growth factor receptor function. *J Biol Chem* 1997; **272**: 9275–9.
31 Tsuda T, Ikeda Y, Taniguchi N. The Asn-420-linked sugar chain in human epidermal growth factor receptor suppresses ligand-independent spontaneous oligomerization. Possible role of a specific sugar chain in controllable receptor activation. *J Biol Chem* 2000; **275**: 21 988–94.
32 Fernandes H, Cohen S, Bishayee S. Glycosylation-induced conformational modification positively regulates receptor-receptor association: a study with an aberrant epidermal growth factor receptor (EGFRvIII/DeltaEGFR) expressed in cancer cells. *J Biol Chem* 2001; **276**: 5375–83.
33 Selvaggi G, Novello S, Torri V *et al.* Epidermal growth factor receptor overexpression correlates with a poor prognosis in completely resected non-small-cell lung cancer. *Ann Oncol* 2004; **15**: 28–32.
34 Tracy S, Mukohara T, Hansen M, Meyerson M, Johnson BE, Janne PA. Gefitinib induces apoptosis in the EGFRL858R non-small-cell lung cancer cell line H3255. *Cancer Res* 2004; **64**: 7241–4.
35 Chen YR, Fu YN, Lin CH *et al.* Distinctive activation patterns in constitutively active and gefitinib-sensitive EGFR mutants. *Oncogene* 2006; **25**: 1205–15.
36 Sordella R, Bell DW, Haber DA, Settleman J. Gefitinib-sensitizing EGFR mutations in lung cancer activate anti-apoptotic pathways. *Science* 2004; **305**: 1163–7.

GFP image analysis in the mouse orthotopic bladder cancer model

MARCO A. DE VELASCO[1], MOTOYOSHI TANAKA[1], SATOSHI ANAI[3], ATSUSHI TOMIOKA[3], KAZUTO NISHIO[2] and HIROTSUGU UEMURA[1]

Departments of [1]Urology and [2]Genome Biology, Kinki University School of Medicine, 377-2 Ohno-Higashi, Osaka-Sayama, Osaka; [3]Department of Urology, Nara Medical University, 840 Shijo-cho, Kashihara, Nara, Japan

Abstract. Precise and objective measurements of tumor response have yet to be standardized in the mouse orthotopic bladder cancer model. In this study, we used image analysis and green fluorescent protein (GFP) to objectively measure tumor size in response to chemotherapy. KU-7 human bladder cancer cells transfected with GFP were intravesically inoculated into 8-week-old female nude mice. Fourteen days after tumor cell inoculation, the mice were assigned into a control (PBS) group or a doxorubicin (conc. 1.0 mg/ml) treatment group and received a single instillation of treatment. Fourteen days after treatment, the bladders were surgically exposed and fluorescent images were captured and later analyzed using image analysis. Bladders were processed for histological examination. Tumor incidence determined by GFP expression and histology was 100 and 80%, respectively, in the doxorubicin treatment group. A 9-fold (histology) vs. 12-fold (GFP expression) difference in tumor regression measured by tumor area ($P<0.05$) and a 5-fold (histology) vs. 9-fold (GFP expression) difference in tumor regression measured by the percent of tumor area in the bladder ($P<0.001$) were observed in the doxorubicin treatment group. Our findings suggest that using image analysis provides a precise, sensitive and objective means to measure tumor growth and treatment response in the mouse orthotopic bladder cancer model in lieu of histological methods. Consequently, the number of mice required in an experiment can be reduced since tissue samples are not needed for histology, thus making tissue samples readily available for additional assays in both a labor-effective and cost-effective manner.

Correspondence to: Dr Motoyoshi Tanaka, Department of Urology, Kinki University School of Medicine, 377-2 Ohno-Higashi, Osaka-Sayama, Osaka 589-8511, Japan
E-mail: mtanaka@med.kindai.ac.jp

Abbreviations: BCG, Bacille Calmette-Guérin; CCD, charge-coupled device; Dox, doxorubicin; EDTA, ethylenediamine tetra-acetic acid; GFP, green fluorescent protein; H&E, hematoxylin and eosin; PBS, phosphate-buffered saline; PSA, prostate specific antigen; ROI, region of interest

Key words: bladder cancer, green-fluorescent proteins, mouse, computer-assisted image analysis

Introduction

In the United States alone, urinary bladder cancer accounts for over 60,000 new cases per year and in Japan, over 16,000 new cases are reported annually (1,2). In Japan and western countries over 90% of the bladder carcinomas are urothelial carcinomas (3). Transurethral resection in combination with intravesical Bacille Calmette-Guérin (BCG) or chemotherapy are the mainstay for treatment of these lesions; however, 5- and 10-year recurrence rates of over 60 and 90%, respectively, pose a major challenge in the treatment and eradication of disease (3,4). These factors combined necessitate further evaluation of new treatment strategies.

Orthotopic tumor models provide researchers with an invaluable research tool, as tumor cells are able to grow in a native environment that more closely resembles its natural state. The mouse orthotopic bladder cancer model has been used for over 30 years, recently this model was modified by using human bladder cancer cells transfected with green fluorescent protein (GFP) implanted transurethally for *in vivo* visualization of tumor growth (5-7). GFP, a spontaneously fluorescent protein that absorbs UV-blue light and emits green fluorescence, has been shown to be suitable in monitoring and visualizing tumors *in vivo* (8). Additionally, tracking cells that stably express GFP *in vivo* allows for a rapid and more precise method for detecting tumor cells than the more traditional histological methods (9). Orthotopic bladder cancer models have already been used successfully to measure the treatment efficacy in chemotherapy, immunotherapy, gene therapy, and chemoprevention models (10-13). This system provides an ideal setting for testing chemotherapeutic agents *in vivo*; however, the challenge to accurately, practically, and objectively measure tumor response remains. Traditional means to measure tumor response have either been qualitative (rather than quantitative) or subjective. The use of computer assisted image analysis provides a solution to this problem in that it allows for a means to measure data in an unbiased manner. Measurement data can be spatially calibrated and since the manner of analysis is standardized, the results are consistently reproduced.

We propose a model that allows the use of image analysis software to accurately measure the growth and response of orthotopically implanted GFP-labeled human bladder cancer cells to intravesical drug treatment. For this purpose, we used doxorubicin (Dox), an anthracycline antibiotic commonly used in maintenance therapy for superficial bladder cancer (4).

Materials and methods

Bladder cancer cell line and transfection. KU-7, a human bladder cancer cell line derived from a superficial papillary tumor was used for our experiments (14). KU-7 cells were maintained in Gibco DMEM (Dulbecco's modified Eagle's medium) (Invitrogen, Carlsbad, CA) supplemented with 10% fetal calf serum in a 37˚C incubator with 5% CO_2. Stable GFP clones were generated as previously described (7). GFP expression was confirmed under a fluorescence microscope.

Orthotopic tumor implantation and intravesical treatment. Prior to bladder instillation, the cells were trypsinized and re-suspended in serum-free DMEM at a concentration of $1x10^8$ cells/ml. A method for the orthotopic instillation of tumor cells has been described (7). Briefly, eleven 8-week-old female athymic nude mice were anesthetized by intraperitoneal injection with Nembutal (Dainippon Sumitomo Pharma, Osaka, Japan). A 24-gauge catheter was inserted transurethrally into the bladder (Fig. 1A) and washed with 200 μl of PBS (phosphate-buffered saline). The bladder was emptied and 100 μl of 0.2% trypsin in 0.02 EDTA (Invitrogen, Carlsbad, CA) was infused and retained for 20 min. A 100-μl KU-7/GFP cell suspension containing $1x10^7$ cells was instilled into the bladder thereafter. The urethra was then ligated for 2-3 h with a purse-string suture to prevent leakage of tumor cells. Fourteen days after cell implantation, the animals were assigned to a control (PBS) (n=6) or doxorubicin (doxorubicin hydrochloride) (Kyowa Hakko Co. Ltd., Tokyo, Japan) (conc. 1.0 mg/ml) (n=5) treatment group and received a single intravesical treatment instillation that was retained for 1 h by purse-string suture.

In vivo fluorescence analysis of mouse bladders. Twenty-eight days following the instillation of tumor cells, the mice were again anesthetized as previously described and the bladders were surgically exposed. The whole mouse was placed under a Leica MZFL (FLVO III) dissecting stereomicroscope equipped with a fluorescent light source with a GFP2 filter and a CCD camera (Leica Microsystems, Heerbrugg, Switzerland). The exposed bladders were examined under fluorescence for the presence of tumors and digital images were captured under both fluorescent and incandescent light (Fig. 1B-D). The mice were then sacrificed and bladders were removed then fixed in 10% neutral buffered formalin.

Histological examination. The bladders were fixed overnight in 10% neutral buffered formalin and then transferred to 70% ethanol. Bladders were then sliced transversally in half and examined under a stereomicroscope. Tumor presence was confirmed and representative images were captured. The samples were then embedded in paraffin, step-sectioned and stained with hematoxylin and eosin (H&E). Tumors were verified under a light microscope and representative digital images were recorded for subsequent image analysis.

Image analysis. Image analysis was performed with ImageJ public domain software available through the National Institutes of Health (Bethesda, MD; available at http://rsb.info.nih.gov/ij/). All images were spatially calibrated for area measurements. Fig. 2 demonstrates an example of the process used to analyze and measure the bladders and tumors. Images of the processed bladders were captured from H&E stained slides and both the bladder and tumors were traced individually and identified by creating a ROI (region of interest) for each. The area was then calculated for each of the selected ROIs. Multiple step sections were taken from the embedded bladders and sections containing the largest tumor size were used for the area calculations. In cases with multiple tumors, lesions were identified and measured individually, however, the measurement data from multiple tumors in an individual bladder was pooled and the area is represented as a single area measurement.

Statistical analysis. Data were statistically analyzed using the Student's t-test and differences were considered to be significant at $P<0.05$. For comparisons between histological analysis and GFP expression, regression analysis was performed. Statistical analysis was carried out using SigmaStat 3.5 (Systat Software, Inc., Jose, CA).

Results

Tumor incidence. We first measured tumor incidence for the implanted KU-7/GFP cancer cells. To measure tumor incidence by GFP expression, surgically exposed bladders were viewed under blue fluorescent light. Bladders without tumors failed to demonstrate any fluorescence; on the other hand, bladders with tumors expressing GFP were easily identified by green fluorescence. Tumor appearance ranged from small individual nests of cells to multiple clusters and/or large masses (Fig. 3). Tumor incidence is defined as the percentage of mice with visible tumors and was determined by direct observation of positive GFP cells within the bladder *in vivo* and/or the presence of tumor cells in the bladder by histological examination. Tumor incidence measured by GFP expression was 100% for all mice in the control and doxorubicin groups. Tumor incidence measured by histological analysis was 100% for the control group but 80% for the doxorubicin treatment group. Histological analysis for tumor incidence failed to reveal microscopic lesions that were clearly detectable by GFP fluorescence.

Measurements of tumor area. Next, we confirmed that cells emitting the green fluorescence were indeed the KU-7/GFP inoculated. To accomplish this, we examined the H&E stained paraffin sections of bladder tumors and compared them with the *in vivo* GFP image and the image of the transversally sliced gross bladders. Once confirmed, we proceeded to measure the bladders and tumors. Tumor size measurements are represented by tumor area and tumor area percent and were calculated by histological analysis and GFP expression. Tumor area is defined a the area of positive GFP emitting regions of green

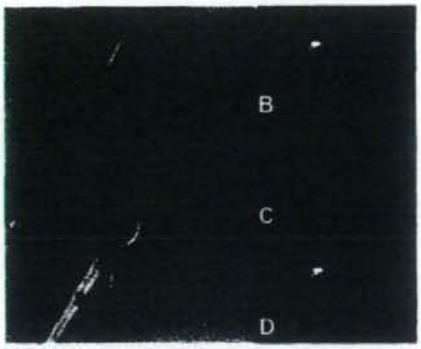

Figure 1. The anatomical view of the nude mouse during the urinary catheterization procedure (A). *In vivo* digital images were obtained by first making a transverse incision across the lower abdomen to expose the bladder. The exposed bladder was filled with PBS an image was acquired using a tungsten light source (B). The bladder was then exposed to a 470-nm wavelength blue light and an image was captured through a 530-nm wavelength emission filter (C). The two images are merged together for the purpose of demonstrating the anatomical location of GFP-labeled tumor cells within the bladder *in vivo* (D).

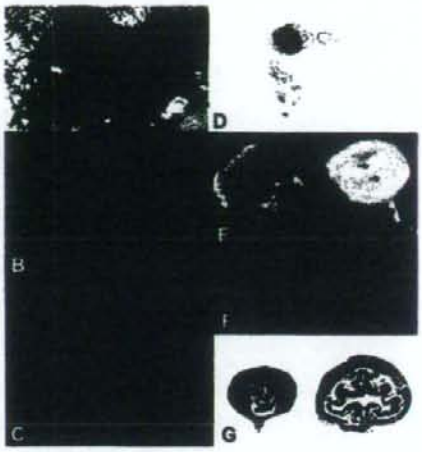

Figure 2. Bladder images were captured under tungsten light (A) and fluorescent light (B) *in vivo*. The raw unmanipulated image was then adjusted and corrected to remove non-specific fluorescence (C). Non-specific fluorescence was subtracted from the background by adjusting contrast and brightness and selecting the appropriate maximum and minimum light and dark set-levels for each individual image. The corrected image was converted to a 16-bit inverted grayscale image, and a mask using color-coded contour lines corresponding to light intensity (corresponding to GFP expression) was applied to identify the tumor (D). Tumor tissue (arrows) was confirmed with the gross bladder (E-F) and the corresponding H&E stained section (G).

fluorescent light in the images captured *in vivo* or regions of tumor bounded by the ROI in selected histological slides. All area measurements are represented by mm^2. To avoid possible differences that may have occurred by having bladders expanded to different diameters, we calculated the tumor area percent. Tumor area percent represents the percent of bladder area comprised of tumor. Regression analysis determined the R^2 values for tumor area and tumor area percent to be 0.281 and 0.692, respectively (Fig. 4). Doxorubicin efficacy against tumor growth resulted in a 9- and 12-fold decrease of tumor area when measured by histological analysis and GFP expression, respectively (Fig. 5A). Similarly, a 5- and 9.25-fold difference in tumor growth was noted when

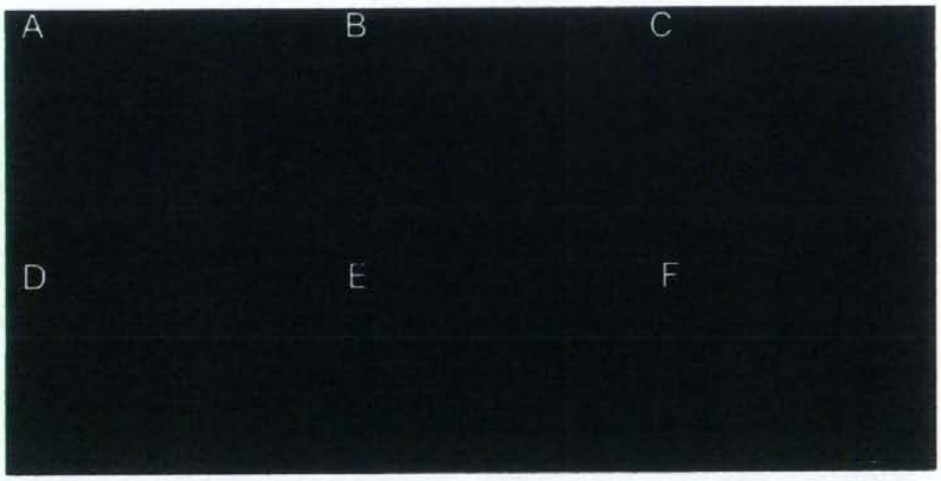

Figure 3. Representative images of bladders taken under a fluorescent light source demonstrate the presence of KU-7/GFP cells by the emission of green fluorescent light. No tumor is present in (A) and as small microscopic lesion is visible (B). Tumors may appear as multiple tumor clusters of varying sizes (C-E) or as a large mass (F).

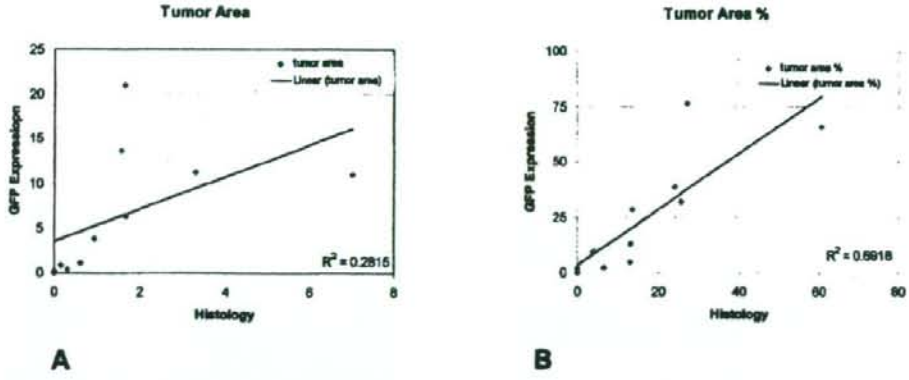

Figure 4. Correlation of tumor area (A) and tumor area percent (B) for all mice bearing KU-7/GFP orthotopic bladder tumors (n=10). GFP expression was plotted against histology examination.

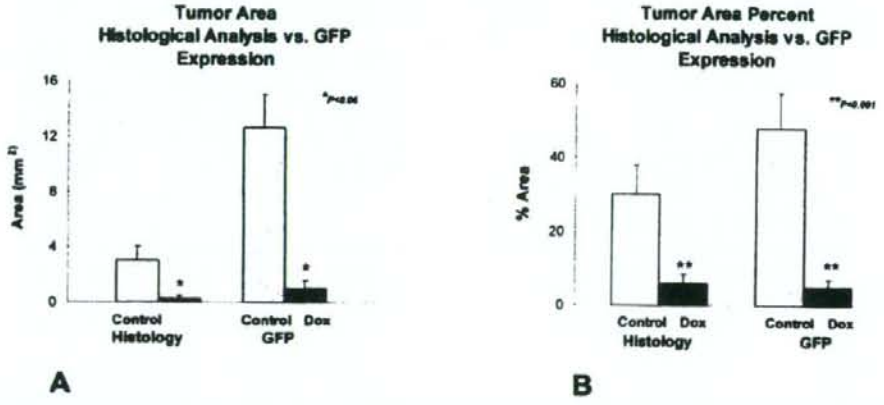

Figure 5. Comparison of tumor response to doxorubicin graphed as tumor area (A) and tumor area percent (B) by GFP expression and histological analysis. *, **P-values versus control, Student's t-test analysis.

measuring tumor response as a percent of the total bladder area as measured by histological analysis and GFP expression, respectively (Fig. 5B).

Although correlation analysis does not demonstrate a strong correlation between tumor sizes measured by GFP and histological analysis, reproducibility and sensitivity were greater by using GFP analysis alone. Similar results were obtained by repeating similar experiments at varying time points (data not shown).

Discussion

The orthotopic bladder cancer model has proven to be one of the most effective models to study tumor biology, particularly in studies involving intravesical therapy. This is due to the fact that tumors are directly exposed to the chemotherapeutic agents in their natural environment (15). Unlike ectopic xenograft models that grow easily visible subcutaneous tumors, bladder orthotopic models grow tumors internally that cannot be visualized grossly *in vivo* and thus renders a challenge to confirm tumor incidence, growth and response. Traditional methods to determine tumor burden in the orthotopic bladder cancer model consist of weighing the bladder and histological analysis (16). However, sensitivity and objectivity in measuring tumor burden is limited due to variability of bladder and tumor size, especially in the case of microscopic disease. Use of GFP-labeled bladder cancer cells in the orthotopic bladder cancer model provides an added means to qualitatively identify such tumors *in vivo*, however, precise and objective quantitative methods have yet to be developed.

The focus of this experiment is to establish a method to measure tumor size in an objective and efficient manner. We compared sensitivity, objectivity and efficiency in measuring tumor response after chemotherapeutic treatment with doxorubicin against the more traditional histological evaluation method. Our results clearly elucidate some of the benefits

gained by using this method versus the more traditional histological method, namely sensitivity and objectivity. This technique allows for a more sensitive and faster method to detect tumor presence in the bladder, especially in cases involving microscopic lesions. Use of image analysis provides not only an objective solution for the interpretation of visual data; it also allows us to establish a workflow in a convenient and efficient manner (17). Our data suggest that measuring the amount of GFP fluorescence emission is sufficient to determine tumor burden and calculate tumor response to treatment.

In traditional methods, tumor burden is calculated by histological examination (i.e., H&E stained slides) usually examining a single plane of the tumor, thus giving us only a snapshot that may or may not be accurate. Large tumors pose a problem in that they are irregular which may lead to bias when searching for the best representative section to analyze and quantify. Furthermore, small tumors present a different problem in that they may be too small to accurately capture in a thin section and may therefore lead to inaccuracies as they may be missed during routine histological procedures. Another complication is that we attempt to examine a two-dimensional object and interpret it as a three-dimensional structure. These differences are supported by our correlation analysis data of tumor size measurements by GFP emission and histology confirming that these are in fact two separate parameters.

An alternate method used to determine tumor burden in the orthotopic bladder cancer model is weighing the bladder; however, this only compares the bladder of one mouse versus that of other mice (18). The problem with this method is that it does not provide any information pertaining to the location of the lesion or the number of lesions involved. Another method used by some investigators is to measure urine PSA (prostate specific antigen) levels generated by tumors of genetically modified cancer cells to produce PSA (19). An advantage to this method is that it allows for a non-invasive method for the determination of tumor growth, however, it fails to provide any insight into the morphological dynamics including the number of tumors present or tumor distribution and location in the bladder. Use of bioluminescent particles, such as firefly luciferase, coupled with image analysis allow for accurate *in vivo* measurements of labeled tumors (20,21). The drawback to this method is the investment involved as it requires specialized dedicated imaging equipment for imaging small animals.

Our results demonstrate that using computer assisted image analysis to measure GFP expression, as a parameter for the determination tumor response to therapy in the mouse orthotopic bladder model, serves as a powerful and objective tool proving to be more sensitive than histology. Additionally, using this method allows the investigator to conduct more labor-effective and cost-effective experiments with minimal investment. Furthermore, this methodology is not limited to the orthotopic bladder cancer model as it can be applied to other tumor models requiring precise objective quantitative analysis of tumor size.

References

1. Jemal A, Siegel R, Ward E, *et al*: Cancer Statistics, 2006. CA Cancer J Clin 56: 106-130, 2006.
2. Cancer Statistics in Japan 2005; Foundation for the Promotion of Cancer Research (http://www.fpcr.or.jp/publication/pdf/statistics 2005.pdf).
3. Kakizoe T: Development and progression of urothelial carcinoma. Cancer Sci 97: 821-828, 2006.
4. Amling CL: Diagnosis and management of superficial bladder cancer. Curr Probl Cancer 25: 224-278, 2001.
5. Soloway MS, De Kernion JB, Rose D, *et al*: Effect of chemotherapeutic agents on bladder cancer: a new animal model. Surg Forum 24: 542-544, 1973.
6. Watanabe T, Shinohara N, Sazawa A, *et al*: An improved intravesical model using human bladder cancer cell lines to optimize gene and other therapies. Cancer Gene Ther 7: 1575-1580, 2000.
7. Zhou JH, Rosser CJ, Tanaka M, *et al*: Visualizing superficial human bladder cancer cell growth *in vivo* by green fluorescent protein expression. Cancer Gene Ther 8: 681-686, 2002.
8. Tanaka M, Gee JR, De la Cerda J, *et al*: Noninvasive detection of bladder cancer in an orthotopic murine model with green fluorescence protein cytology. J Urol 3: 975-978, 2003.
9. Caceres G, Zhu XY, Jiao JA, *et al*: Imaging of luciferase and GFP-transfected human tumours in nude mice. Luminescence 24: 218-223, 2003.
10. Nogawa M, Yuasa T, Kimura S, *et al*: Intravesical administration of small interfering RNA targeting PLK-1 successfully prevents the growth of bladder cancer. J Clin Invest 115: 978-985, 2005.
11. Brocks CP, Buttner H and Bohle A: Inhibition of tumor implantation by intravesical gemcitabine in a murine model of superficial bladder cancer. J Urol 174: 1115-1118, 2005.
12. Wu Q, Mahendran R and Esuvaranathan K: Nonviral cytokine gene therapy on an orthotopic bladder cancer model. Clin Cancer Res 9: 4522-4528, 2003.
13. Singh AV, Franke AA, Blackburn GL and Zhou JR: Soy phytochemicals prevent orthotopic growth and metastasis of bladder cancer in mice by alterations of cancer cell proliferation and apoptosis and tumor angiogenesis. Cancer Res 66: 1851-1858, 2006.
14. Tazaki H and Tachibana M: Studies on KU-1 and KU-7 cells as an *in vitro* model of human transitional cell carcinoma of urinary bladder. Hum Cell 1: 78-83, 1988.
15. Oliveira PA, Colaco A, De la Cruz, *et al*: Experimental bladder carcinogenesis-rodent models. Exp Oncol 28: 2-11, 2006.
16. Hegele A, Dalpke A, Heeg K, *et al*: Immunostimulatory CpG oligonucleotides reduce tumor burden after intravesical administration in an orthotopic murine bladder cancer model. Tumour Biol 26: 274-280, 2005.
17. Hoffman RM: Imaging tumor angiogenesis with fluorescent proteins. APMIS 112: 441-449, 2004.
18. Gunther JH, Frambach M, Deinert I, *et al*: Effects of acetylic salicylic acid and pentoxifylline on the efficacy of intravesical BCG therapy in orthotopic murine bladder cancer (MB49). J Urol 161: 1702-1706, 1999.
19. Wu Q, Esuvaranathan K and Mahendran R: Monitoring the response of orthotopic bladder tumors to granulocyte macrophage colony-stimulating factor therapy using the prostate-specific antigen gene as a reporter. Clin Cancer Res 10: 6977-6984, 2004.
20. Ponomarev V, Doubrovin M, Serganova I, *et al*: A novel triple-modality reporter gene for whole-body fluorescent, bioluminescent, and nuclear noninvasive imaging. Eur J Nucl Med Mol Imaging 31: 740-751, 2004.
21. Yanagihara K, Takigahira M, Takeshita F, *et al*: A photon counting technique for quantitatively evaluating progression of peritoneal tumor dissemination. Cancer Res 66: 7532-7539, 2006.

EphA4 promotes cell proliferation and migration through a novel EphA4-FGFR1 signaling pathway in the human glioma U251 cell line

Junya Fukai,[1,2] Hideyuki Yokote,[2,4] Ryuya Yamanaka,[3] Tokuzo Arao,[4] Kazuto Nishio,[2,4] and Toru Itakura[1]

[1]Department of Neurological Surgery, Wakayama Medical University, Wakayama, Japan; [2]Shien-Lab, National Cancer Center Hospital, Tokyo, Japan; [3]Research Center of Innovative Cancer Therapy, Kurume University School of Medicine, Fukuoka, Japan; and [4]Department of Genome Biology, Kinki University School of Medicine, Osaka, Japan

Abstract

The Eph receptor tyrosine kinases and their ephrin ligands form a unique cell-cell contact-mediated bidirectional signaling mechanism for regulating cell localization and organization. High expression of Eph receptors in a wide variety of human tumors indicates some roles in tumor progression, which makes these proteins potential targets for anticancer therapy. For this purpose, we did gene expression profiling for 47 surgical specimens of brain tumors including 32 high-grade glioma using a microarray technique. The analysis, focused on the receptor tyrosine kinases, showed that EphA4 mRNA in the tumors was 4-fold higher than in normal brain tissue. To investigate the biological significance of EphA4 overexpression in these tumors, we analyzed EphA4-induced phenotypic changes and the signaling mechanisms using human glioma U251 cells. EphA4 promoted fibroblast growth factor 2-mediated cell proliferation and migration accompanied with enhancement of fibroblast growth factor 2-triggered mitogen-activated protein kinase and Akt phosphorylation. In addition, active forms of Rac1 and Cdc42 increased in the EphA4-overexpressing cells. Furthermore, we found that EphA4 formed a heteroreceptor complex with fibroblast growth factor receptor 1 (FGFR1) in the cells and that the EphA4-FGFR1 complex potentiated FGFR-mediated downstream signaling. Thus, our results indicate that EphA4 plays an important role in malignant phenotypes of glioblastoma by enhancing cell proliferation and migration through accelerating a canonical FGFR signaling pathway. [Mol Cancer Ther 2008;7(9):2768–78]

Received 11/7/07; revised 6/18/08; accepted 6/19/08.

Grant support: Third-Term Comprehensive 10-Year Strategy for Cancer Control and Health and Labour Sciences Grants, Research on Advanced Medical Technology, H17-Pharmaco-006.

The costs of publication of this article were defrayed in part by the payment of page charges. This article must therefore be hereby marked *advertisement* in accordance with 18 U.S.C. Section 1734 solely to indicate this fact.

Note: Microarray analyses were carried out using BRB Array Tools developed by Dr. Richard Simon and Amy Peng. K. Nishio and T. Itakura designed the research, J. Fukai and H. Yokote did the research, R. Yamanaka and T. Arao contributed to data analysis, and J. Fukai wrote the article.

Requests for reprints: Kazuto Nishio, Department of Genome Biology, Kinki University School of Medicine, 377-2 Ohno-Higashi, Osaka-Sayama, Osaka 859-8511, Japan. Phone: 81-72-366-0221; Fax: 81-72-366-0206. E-mail: knishio@med.kindai.ac.jp

doi:10.1158/1535-7163.MCT-07-2263

Introduction

The Eph receptors represent the largest family of receptor protein tyrosine kinases and interact with their ligands, ephrins. The Eph receptors and ephrins are divided into two subclasses, A and B, based on their homologies, structures, and binding affinities (1). Fourteen Eph receptors and eight ephrin ligands have been identified thus far in mammals (2–4). Ephrin-A ligands are anchored to the plasma membrane by a glycosylphosphatidylinositol modification. Ephrin-B ligands have a transmembrane domain and a short cytoplasmic tail. The Eph-ephrin system relays a direct cell-cell contact-mediated bidirectional signaling pathway (5, 6). This bidirectional signaling is fundamentally involved in developmental processes (7–9) or in the remodeling of blood vessels (10, 11). Eph-ephrin signaling mainly affects the cell shape and motility by regulating cytoskeletal organization and cell adhesion and also influences cell proliferation and cell-fate determination (3). Therefore, it is speculated that Eph signaling could play some roles in tumorigenesis as one of their possible consequences.

More recently, the genes for Eph receptors and ephrins have been recognized to be differentially expressed in various human tumors including malignant melanoma, glioma, prostate cancer, breast cancer, small cell lung cancer, endometrial cancer, esophageal cancer, gastric cancer, and colorectal cancer (12–18). Profound distortion of expression patterns could be correlated with altered tumor behavior such as increased invasiveness or increased metastatic potential and consequently with poor patient outcome. Despite the widely observed phenomenon of Eph receptor overexpression, their role has not been fully elucidated in the process of malignant phenotypes. However, recent bodies of evidence have implicated Eph involvement in the tumor progression of human cancers including malignant gliomas (19, 20).

The fibroblast growth factor receptor (FGFR) also belongs to a family of receptor protein tyrosine kinases and consists of four members, FGFR1, FGFR2, FGFR3, and FGFR4. At the present, 23 FGF ligands have been cloned and known to bind to and activate FGFRs with their different affinities (21). The FGFR-associated substrate 2α (FRS2α) is a docking